EUROPEAN ORGANIZATION FOR NUCLEAR RESEARCH

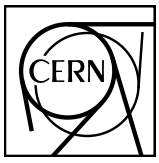

ALICE-INT-2012-xxx
August 23, 2013

Two-proton correlations in Pb–Pb collisions at $\sqrt{s_{\mathrm{NN}}} = 2.76$ TeV from the ALICE experiment at the LHC

Maciej Szymański[1]
Adam Kisiel[1]

1. Warsaw University of Technology

Email: Maciej.Szymanski@cern.ch
Adam.Kisiel@cern.ch

Abstract

Correlations of all combinations of pairs of protons and antiprotons are measured in Pb–Pb collisions at $\sqrt{s_{\mathrm{NN}}} = 2.76$ TeV in the ALICE experiment. One-dimensional pp, $\bar{\mathrm{p}}\bar{\mathrm{p}}$ and $\mathrm{p}\bar{\mathrm{p}}$ correlation functions are formed in three centrality and two pair transverse momentum ranges. The femtoscopic parameters for the radius of the proton source are extracted. The fit includes final-state interactions (strong and Coulomb) and quantum statistics, in case of identical pairs of (anti)protons. Also, the fit takes into account residual correlations coming from pΛ system. Two-proton correlations show an increase of the radius with increasing multiplicity and slight decrease of the radius with increasing pair transverse momentum.

Contents

1 Introduction

In the analysis, we present the measurements of two-proton correlations in Pb–Pb collisions at $\sqrt{s_{\rm NN}} =$ 2.76 TeV registered by the ALICE experiment. The method of two-particle correlations (commonly referred to as *femtoscopy*) allows for extracting the space-time characteristics of the emitting source created in heavy-ion collision. Correlations of identical bosons have been usually used to perform this study. In particular, the ALICE Collaboration has recently carried out the analysis of two-pion correlations in central Pb–Pb collisions [1]. Proton-proton correlations have also been measured for the broad range of the energies of heavy-ion collisions, especially in Au+Au collisions at $\sqrt{s_{\rm NN}} = 200$ GeV by the STAR experiment at RHIC [2].

The main motivation to carry out two-proton femtoscopic study is to complement information about the source size deduced from the correlations of pions and kaons. The analysis provides a test of the hydrodynamic prediction of the transverse mass scaling and gives a possibility for checking if the collectivity also includes baryons. Due to the fact that feed-down from weak decays cannot be neglected in high-energy heavy-ion collisions, the effects of residual correlations related with the pΛ system should be taken into account in the study of proton femtoscopy. Because of the low decay momentum of Λ decay into p and π^- with respect to the mass of proton, femtoscopic correlations between a Λ and a primary proton might still be detected for a pair consisting of a primary proton and the proton from Λ. Furthermore, proton-antiproton correlations should be investigated as a proof that the influence of final-state interaction (the annihilation) may contribute to lowering multiplicities of protons observed at LHC energies, with respect to predictions from chemical models.

2 Data analysis

2.1 Data sample

2.1.1 Collision data

The data used in this note come from Pb–Pb collisions recorded by the ALICE experiment during the 2011 run at the LHC (production LHC11h, pass 2). Analysis Object Data (AOD115) files have been used in studies. About 35 milion events have been analysed. The following runs have been used (they correspond to the uniform acceptance - LHC11h_AOD115_fullTPCFlow dataset from CF_PbPb analysis train):

167915, 168115, 168460, 169035, 169238, 169859, 170228 , 167920, 168310, 168464, 169091, 169411, 169923, 170230, 167985, 168311, 168467, 169094, 169415, 170027, 170268, 167987, 168322, 168511, 169138, 169417, 170081, 170269, 167988, 168325, 168512, 169144, 169835, 170155, 170270, 168069, 168341, 168514, 169145, 169837, 170159, 170306, 168076, 168342, 168777, 169148, 169838, 170163, 170308, 168105, 168361, 168826, 169156, 169846, 170193, 170309, 168107, 168362, 168988, 169160, 169855, 170203, 168108 , 168458, 168992, 169167, 169858, 170204.

Also, the data collected in the 2010 were used for comparison. The following runs have been used (LHC10h_AOD086 dataset from CF_PbPb analysis train):

139510, 139507, 139505, 139503, 139465, 139438, 139437, 139360, 139329, 139328, 139314, 139310, 139309, 139173, 139107, 139105, 139038, 139037, 139036, 139029, 139028, 138872, 138871, 138870, 138837, 138732, 138730, 138666, 138662, 138653, 138652, 138638, 138624, 138621, 138583, 138582, 138579, 138578, 138534, 138469, 138442, 138439, 138438, 138396, 138364, 138275, 138225, 138201, 138197, 138192, 138190, 137848, 137844, 137752, 137751, 137724, 137722, 137718, 137704, 137693, 137692, 137691, 137686, 137685, 137639, 137638, 137608, 137595, 137549, 137544, 137541, 137539, 137443, 137441, 137440, 137439, 137434, 137432, 137431, 137430, 137366, 137243, 137236, 137235, 137232, 137231, 137230, 137162, 137161, 137135

The analysis was done as a part of the "Lego Trains".

2.1.2 Monte Carlo

We used the HIJING production LHC11a10a_bis (AOD120) and AMPT production LHC12a17a (AOD110).

2.2 Analysis software

The analysis was performed using the `AliFemto` package being a part of `AliROOT` framework (v5-03-34-AN):

`http://alisoft.cern.ch/viewvc/tags/v5-03-34-AN/PWGCF/FEMTOSCOPY/`.

Measured correlation functions have been fitted with the custom written software. It required the input from `THERMINATOR` model [3], which is a particle and event generator basing on Monte Carlo methods. The model aims to study particle production in relativistic heavy ion collisions at the energies available at RHIC and LHC. `THERMINATOR` uses the statistical approach to describe particle production. Also, the chemical and kinetic freeze-out are assumed to occur simultaneously (*single freeze-out model*).

The fitting program makes also use of theoretical pp and pΛ correlation functions. The former one is calculated with `CorrFit` software [4], which compares the measured correlation function and a model one calculated using Lednicky's weights, experimental distribution of particles' momenta and an assumed emission source distribution via χ^2 test in the given range of fitting parameters. The latter one is obtained from the analytical formula of Lednicky [5], which uses the parametrization of strong interaction for pΛ system. The correlation function is calculated as the square of the wave function averaged over the total spin and over the assumed gaussian distribution of the relative distance between particle emission points in the pair rest frame.

2.3 Event selection

Events for the analysis were selected using minimum bias (kMB), central (kCentral) and semicentral (kSemiCentral) triggers. Events were required to have the collision vertex position within ± 8 cm from the centre of TPC, measured along the beam axis. The centrality selection classes are used to determine the centrality with the V0.

2.4 Particle identification

The analysis of pion femtoscopy in Pb–Pb collisions has shown that there is a need to use the so-called *TPC-only tracks* constrained to the SPD vertex (with AOD filter bit 7 set). The main reason for this is related to the fact that global tracking forces some pairs of tracks to have very similar momenta that leads to distortions in the shape of correlation functions for the lowest values of the momentum difference and, as a consequence, incorrect extracted source radii [6]. It has also been shown that the *number of* $\sigma's$ method gives more pure sample of particles than the Bayesian PID method [8]. However, *TPC-only tracks* in the AOD data files have only Bayesian PID and there is not enough information to use the $n\sigma$ method (e.g. TPC and TOF signals are missing). The solution of the above problem [7] is as follows: in AOD files, each *TPC-only track* has its equivalent amongst *global tracks* (having very similar parameters) related by:

```
tpcOnlyTrack->GetID() = - 1 - globalTrack->GetID().
```

Hence, there is a need to loop over all *global tracks* to save their indices and IDs. Afterwards, in a loop over *TPC-only tracks*, one is able to get directly a *global track* which corresponds to the current *TPC-only track* and copy the PID information. This procedure was implemented as a part of the `AliFemto` package. Femtoscopy analysis requires as pure sample of particles as possible but also high statistics of

them. A combined TPC and TOF method was applied to select (anti)protons. The details of the cut are as follows:

- for tracks momenta less than 0.8 GeV/c: $n\sigma_{TPC} < 3$
- for tracks momenta higher than 0.8 GeV/c: $\sqrt{n\sigma_{TPC}^2 + n\sigma_{TOF}^2} < 3$

PID purity was estimated with MC simulations (HIJING). Results are summarized in Tab. 1

	HIJING		AMPT	
	p	$\bar{p}$	p	$\bar{p}$
protons	95.7%	95.9%		
kaons	1.9%	1.4%		
pions	0.9%	1.0%		
muons	0%	0%		
electrons	1.5%	1.7%		

Table 1: Proton and antiproton PID purities estimated from MC simulations.

Fig. 1 show QA of PID.

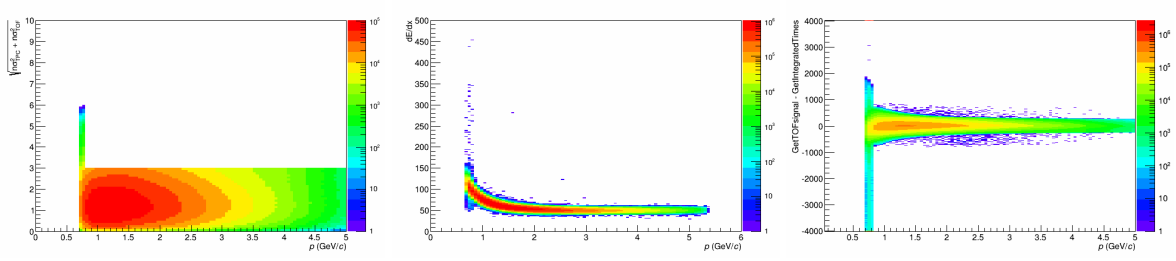

Fig. 1: Left plot: combined TPC and TOF nσ separation vs. momentum for proton mass hypothesis of accepted tracks. Middle plot: dE/dx signal from TPC. Right plot: signal from TOF.

2.5 Track selection

Tracks within the pseudorapidity range $|\eta| < 0.8$ have been selected. We have chosen (anti)protons with $0.7 < p_{\mathrm{T}} < 4.0$ GeV/c. The minimum number of TPC clusters corresponding to the given track was set to 80 (out of all 159 clusters). The maximum value of χ^2 per TPC cluster was 4.0 (2 degrees of freedom per cluster). Fig. 2 shows QA plots of the accepted tracks.

Furthermore, the standard TPC-only track cuts on a Distance of Closest Approach (DCA) was applied: $DCA_{xy} < 2.4cm$ and $DCA_{xy} < 3.2cm$. In previous studies, to calculate DCA values, we used `PropagateToDCA` method applied for the *global tracks* corresponding to *TPC-only tracks* (similarly as with PID) because of better resolution. The comparison of the DCA distribution in the transverse plane for *TPC-only tracks* and *global tracks* is shown in Fig. 4.

However, it caused the unexpected shape of proton-proton correlation functions.

DCA distributions for TPC-only tracks accepted for the analysis are shown in Fig. 4

The contamination from secondary particles ((anti)protons from weak decays and protons produced by interactions of particles with detector material) was estimated using MC (HIJING, LHC11a10a_bis, AOD120). It was done using DCA information from global tracks corresponding to TPC-only tracks. Fig. 5 shows DCA_{xy} template distributions of protons and antiprotons: for primary particles, particles

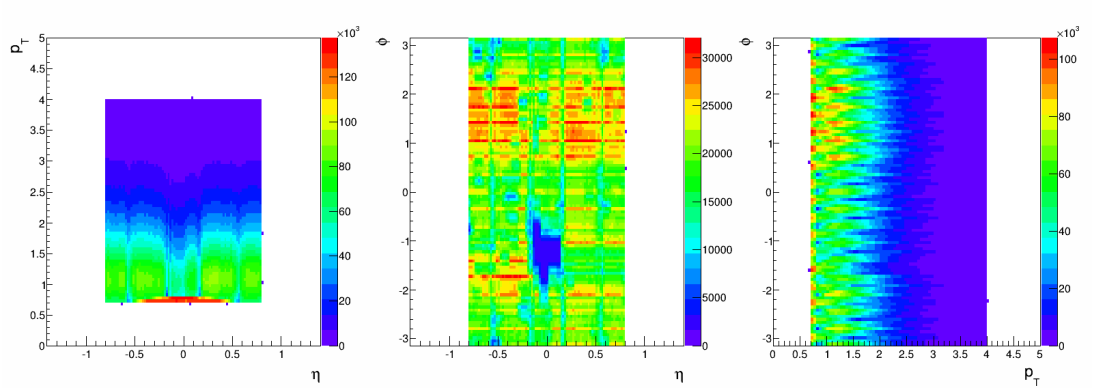

Fig. 2: QA histograms of accepted tracks.

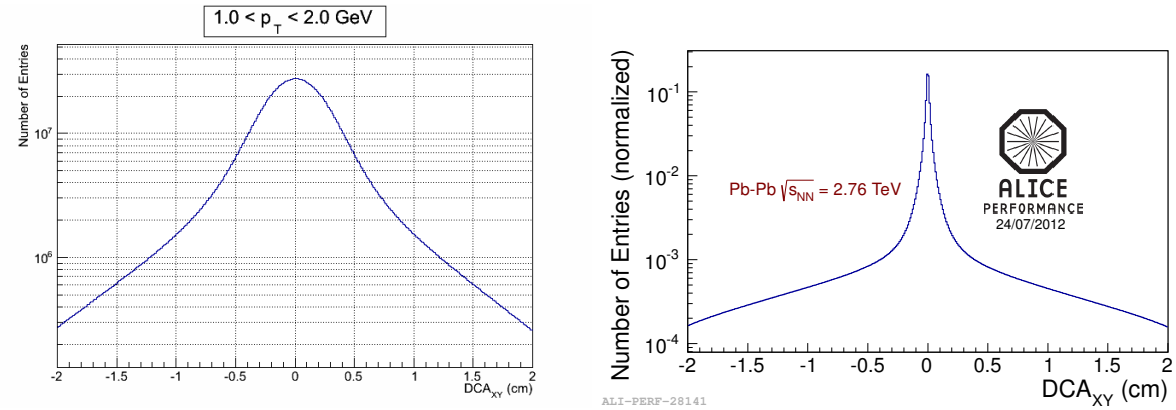

Fig. 3: The comparison of the DCA distribution in the transverse plane for *TPC-only tracks* (left panel) and *global tracks* (right panel).

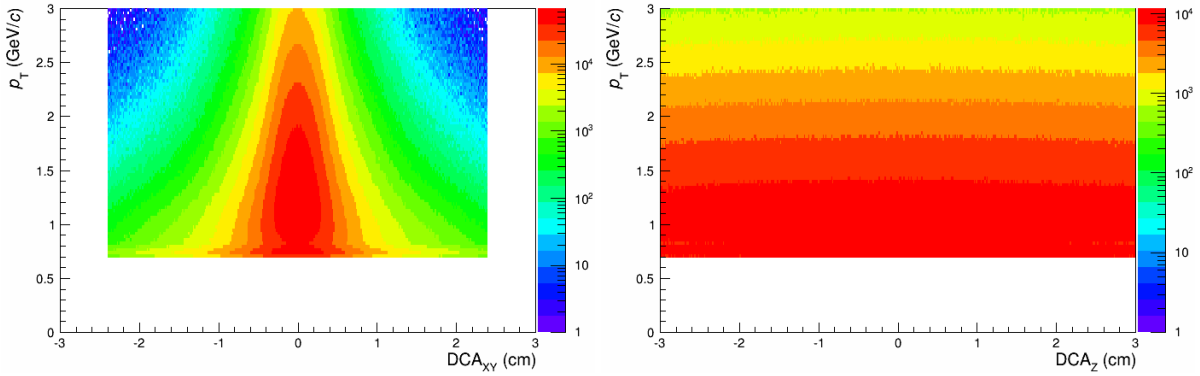

Fig. 4: DCA distribution of accepted tracks in the transverse plane (left panel) and in z direction (right panel).

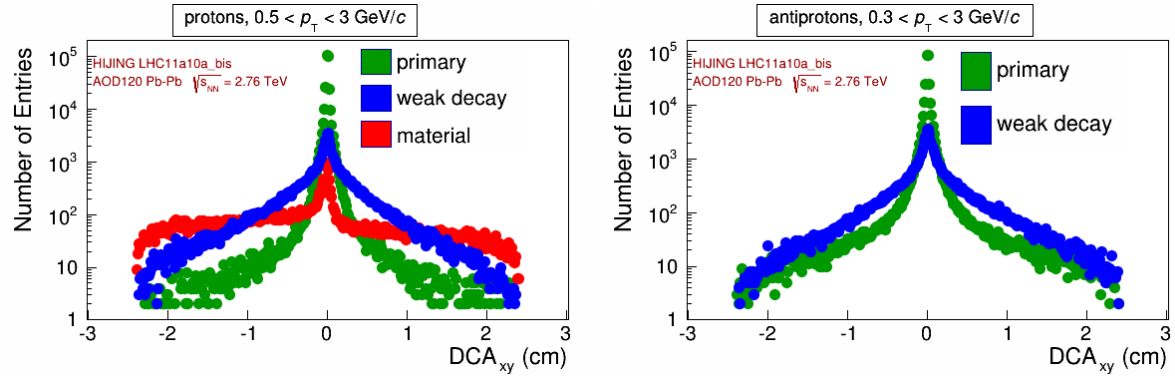

Fig. 5: The DCA_{xy} (for global tracks) template distributions of protons (left plot) and antiprotons (right plot) with respect to theirs origin.

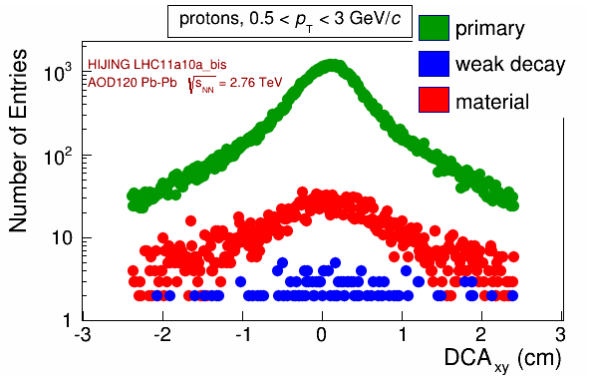

Fig. 6: The DCA_{xy} (for TPC-only tracks) template distributions of protons with respect to theirs origin.

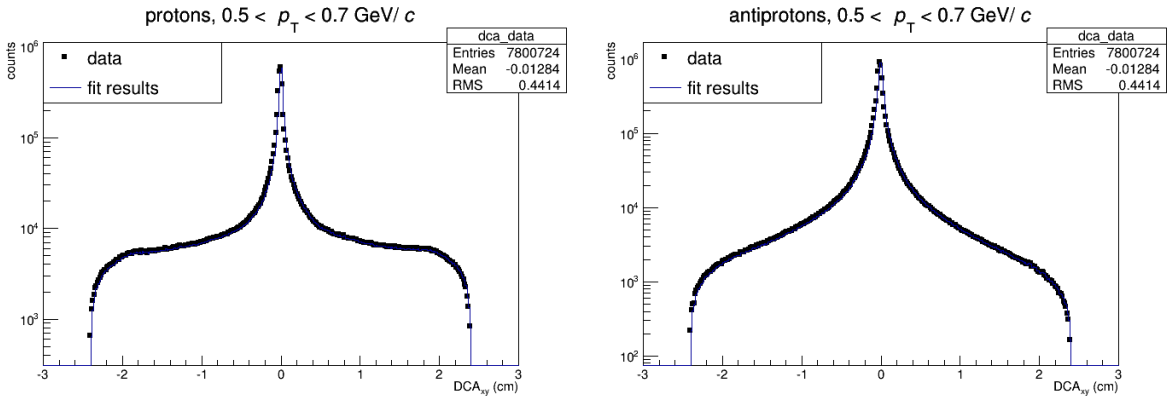

Fig. 7: Examples of fit of DCA_{xy} distributions with MC templates.

from weak decays and particles from material (there was also non-zero fraction of antiprotons "from material", but they are not shown and were excluded from the fitting procedure). Templates obtained for TPC-only tracks are shown in Fig. 6. Similar shapes of all contribution make the relaible fitting impossible.

To calculate the relative contribution of each source of contamination, the data distribution is fitted in [-2.4;2.4]cm range with the template distributions in p_T bins (10 for protons, 11 for antiprotons). The fit was done using TFractionFitter class from ROOT. Examples of fits are shown in Fig. 7.

Results of the fits are shown in Fig. 8.

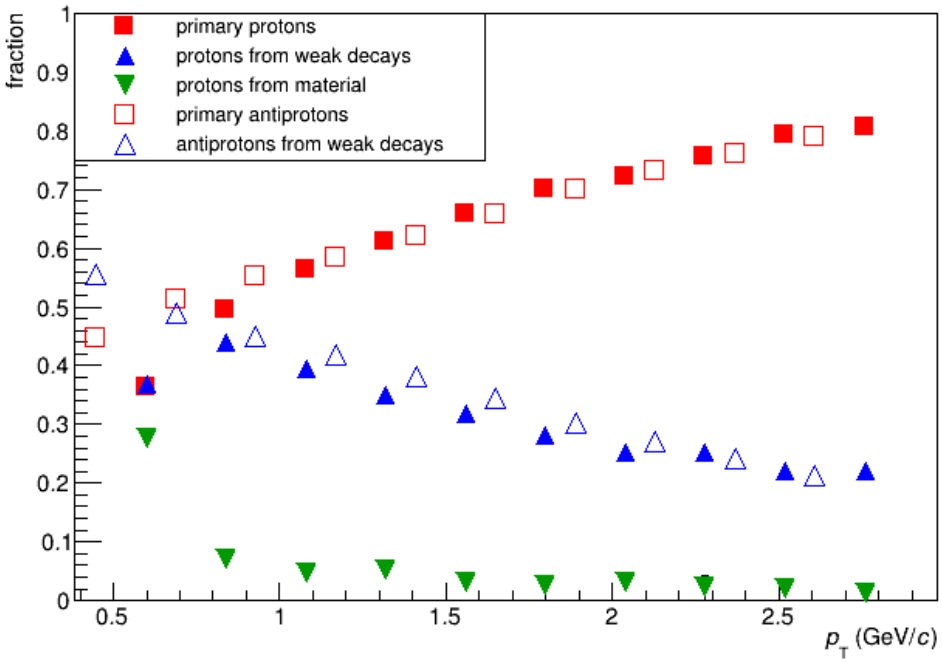

Fig. 8: Fractions of (anti)protons with respect to theirs origin obtained from MC template fits.

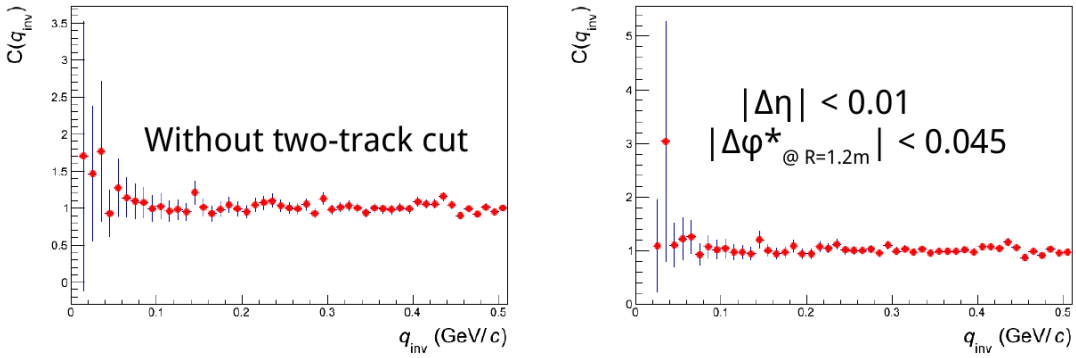

Fig. 9: pp correlation function from HIJING simulations without the cut on angular distance (left panel) and with the cut $|\Delta\varphi^*_{@R=1.2m}| < 0.045$, $|\Delta\eta| < 0.01$ (right panel).

2.6 Pair selection

In case of pair selection criteria, standard cuts preventing the effects of merging (two tracks reconstructed as one) and splitting (one track reconstructed as two) were used. Strictly speaking, the cuts consists of two steps: *share quality* and *share fraction*. The former one bases on the calculation of the fraction of the number of clusters on the same TPC pad row shared by both tracks to the number of all clusters of the two tracks. Maximum *share quality* was set to 1.0 which means accepting all pairs. As regards *share fraction*, it is obtained as a ratio of shared clusters to all clusters of both tracks. All pairs sharing more than 5% clusters were rejected. The cut on angular distance [9] have been applied. Fig. 9 shows proton-proton correlation function from HIJING before and after applying the cut. Only pairs within $|\Delta\varphi^*_{@R=1.2m}| < 0.045$, $|\Delta\eta| < 0.011$) are accepted. Angular distance $|\Delta\varphi^*| = \varphi_1 - \varphi_2 + \arcsin(\frac{eBR}{2p_{T1}}) - \arcsin(\frac{eBR}{2p_{T1}})$, where φ - azimuthal angle of the track at the vertex, e - elementary charge (-0.3 in Heaviside-Lorentz units), B - magnetic field, R - radius in TPC, p_T - transverse momentum , is calculated for TPC radius $R = 1.2\ m$.

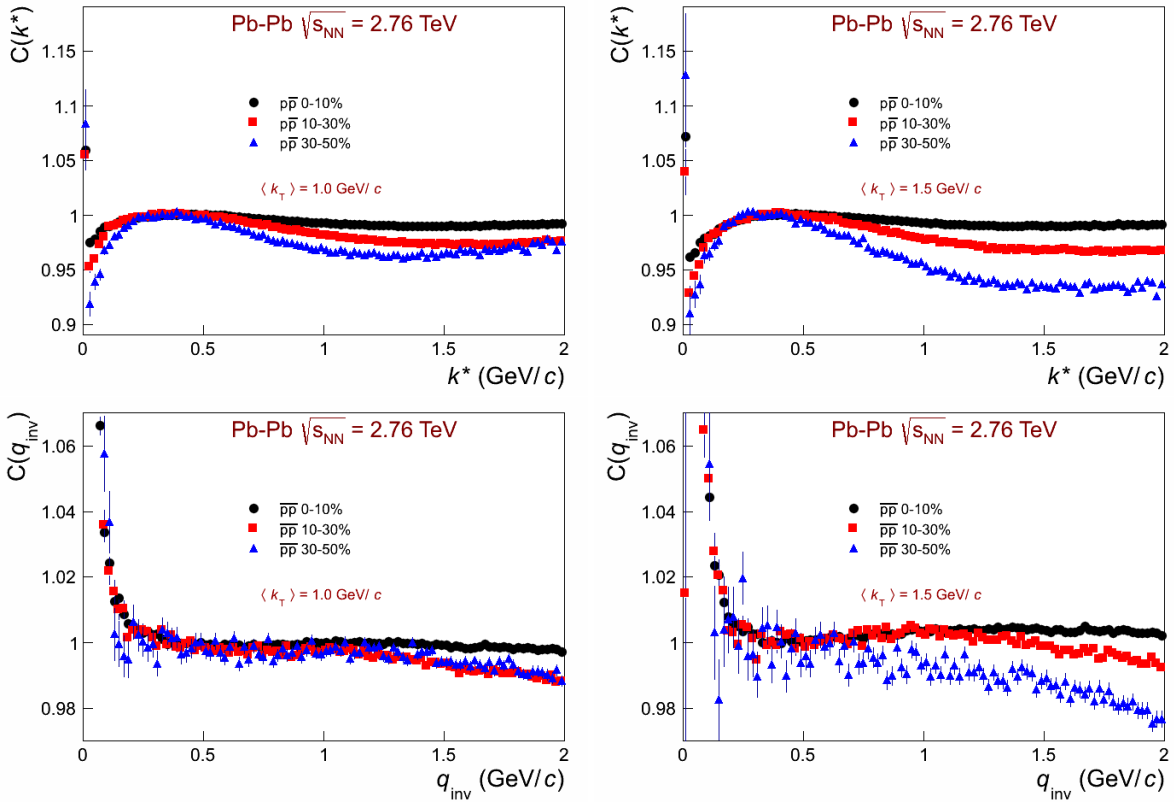

Fig. 10: Proton-antiproton and antiproton-antiproton correlation functions for the $\sqrt{s_{\rm NN}} = 2.76$ TeV Pb–Pb in wide q range.

2.7 Correlation functions

Two-particle correlations were studied in one dimensional representation with respect to the relative momentum $q_{\rm inv} = 2 \cdot k^* = \sqrt{(p_1 - p_2)^2 - (E_1 - E_2)^2}$. The correlation effect was measured with the function defined as:

$$C(q_{\rm inv}) = \frac{A(q_{\rm inv})}{B(q_{\rm inv})}, \tag{1}$$

where $A(q_{\rm inv})$ is a distribution of correlated pairs of particles (coming from the same event), $B(q_{\rm inv})$ is a distribution of uncorrelated pairs of particles (coming from different events - 10 events were used to create the background distribution).

The analysis has been performed for six centrality bins ($0-5\%$, $5-10\%$, $10-20\%$, $20-30\%$, $30-40\%$, $40-50\%$) and then merged into three classes: $0-10\%$, $10-30\%$ and $30-50\%$. Also, correlation functions have been calculated for two bins of the pair transverse momentum $k_{\rm T} = (|\vec{p}_{\rm T,1} + \vec{p}_{\rm T,2}|)/2$: $0.01 < k_{\rm T} < 1.00$ GeV/c and $1 < k_{\rm T} < 5$ GeV/c.

3 Results

3.1 Investigation of non-flat background of correlation function at large q

In Fig. 10 and 11 one can observe that pp, $\bar{\rm p}\bar{\rm p}$ and p$\bar{\rm p}$ correlation functions at large q deviate from unity. The effect increases with centrality and $k_{\rm T}$. The effect is qualitatively similar for p$\bar{\rm p}$ correlations in MC simulations, despite HIJING at low $k_{\rm T}$.

The analysis was redone calculating numerators and denominators in bins of the event plane angle from VZERO detector (`GetEventplane` method from `AliEventplane` class). To study the effect of mixing

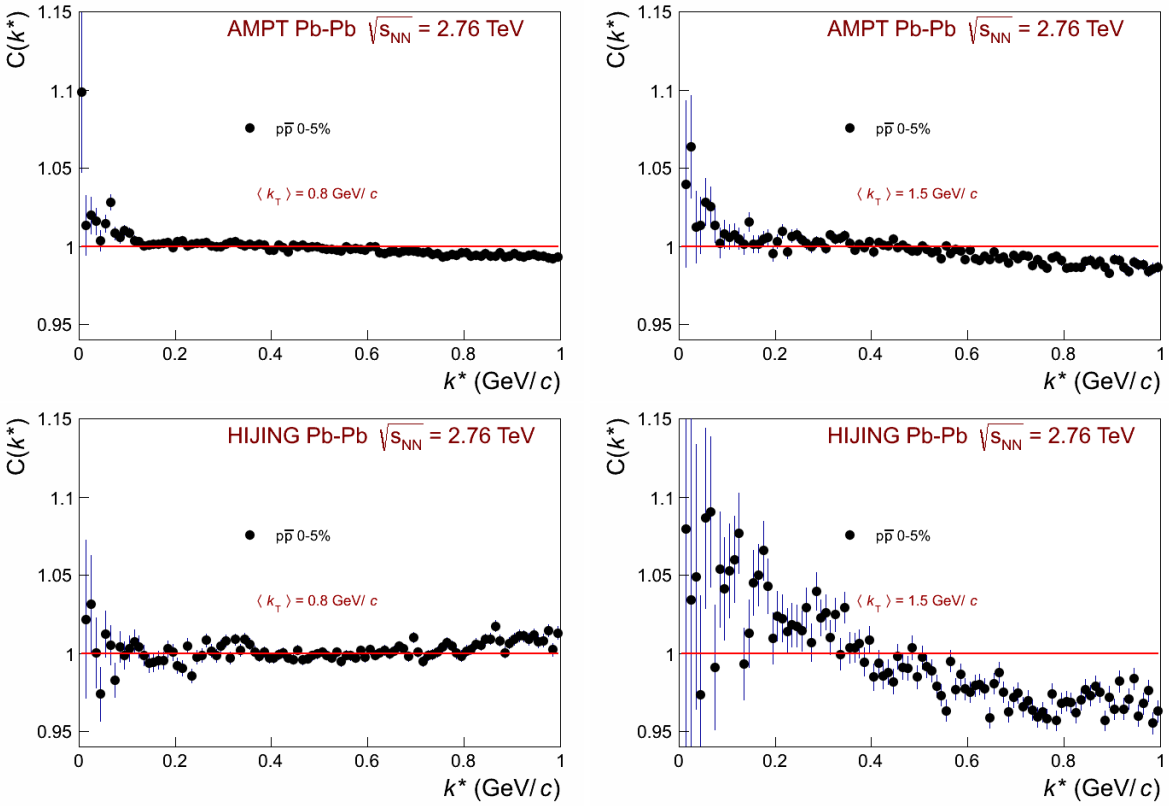

Fig. 11: Proton-antiproton correlation functions for the AMPT and HIJING $\sqrt{s_{\rm NN}} = 2.76$ TeV Pb–Pb in wide q range.

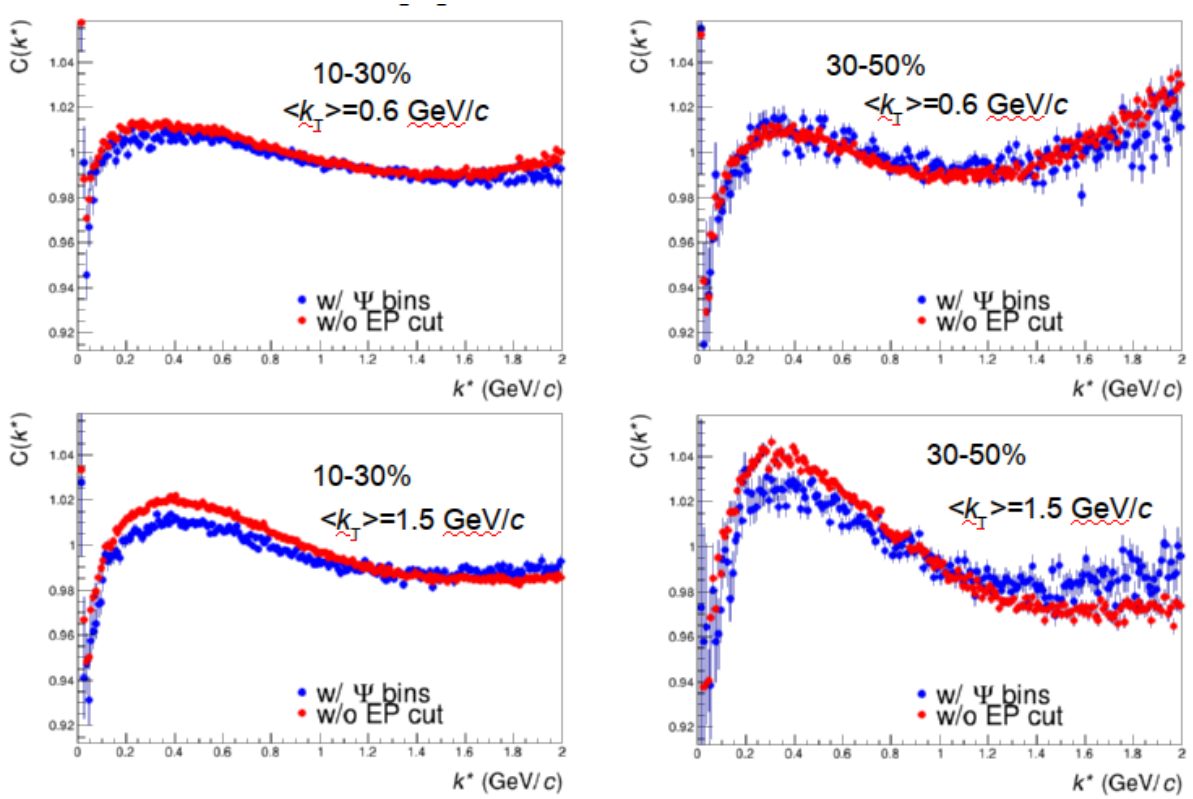

Fig. 12: Comparison proton-antiproton of correlation functions calculated without and with 6 event plane angle selection.

in event plane angle bins on the shape of correlation function at large q, two methods are compared:

- without EP angle selection
  - numerators and denominators from each run added
  - summed numerator divided by summed denominator
  - correlation function scaled by `den->GetEntries()/num->GetEntries()`
- calculations in 6 EP bins, then:
  - numerators from each run and Ψ_2 bin added
  - denominators from each run and Ψ_2 bin scaled by `num[run][psi]->GetEntries()/den[run][psi]->GetEntries()` and then added
  - correlation function: numerator divided by denominator

Results with 6 event plane angle bins are shown in Fig. 12, Fig. 13, Fig. 14. One can notice that the background is slightly more flat in the method with event plane angle binning. However, the effect is rather small, especially for identical pairs.

Results with 3 event plane angle bins are shown in Fig. 15, Fig. 16, Fig. 17. The difference between two methods is much smaller compared to 6-bins case.

Results with 12 event plane angle bins are shown in Fig. 18. The difference between two methods is also smaller compared to 6-bins case.

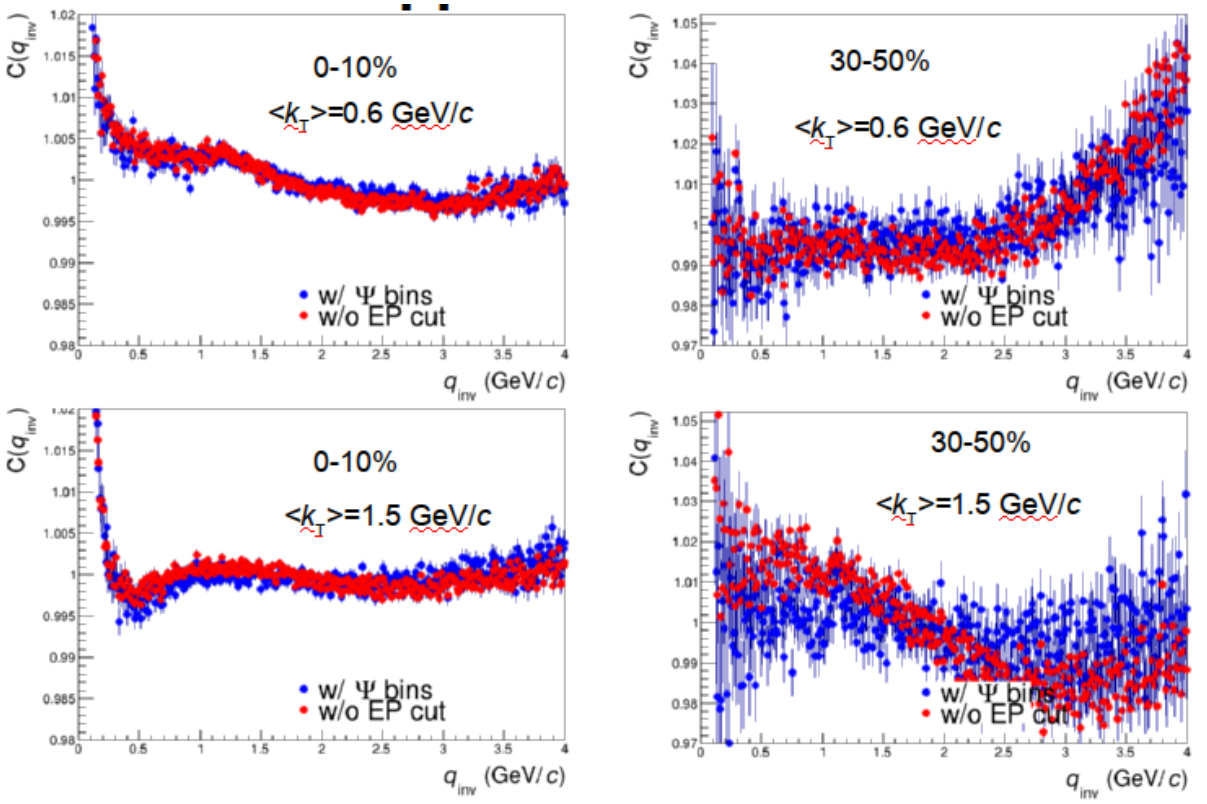

Fig. 13: Comparison of proton-proton correlation functions calculated without and with 6 event plane angle selection.

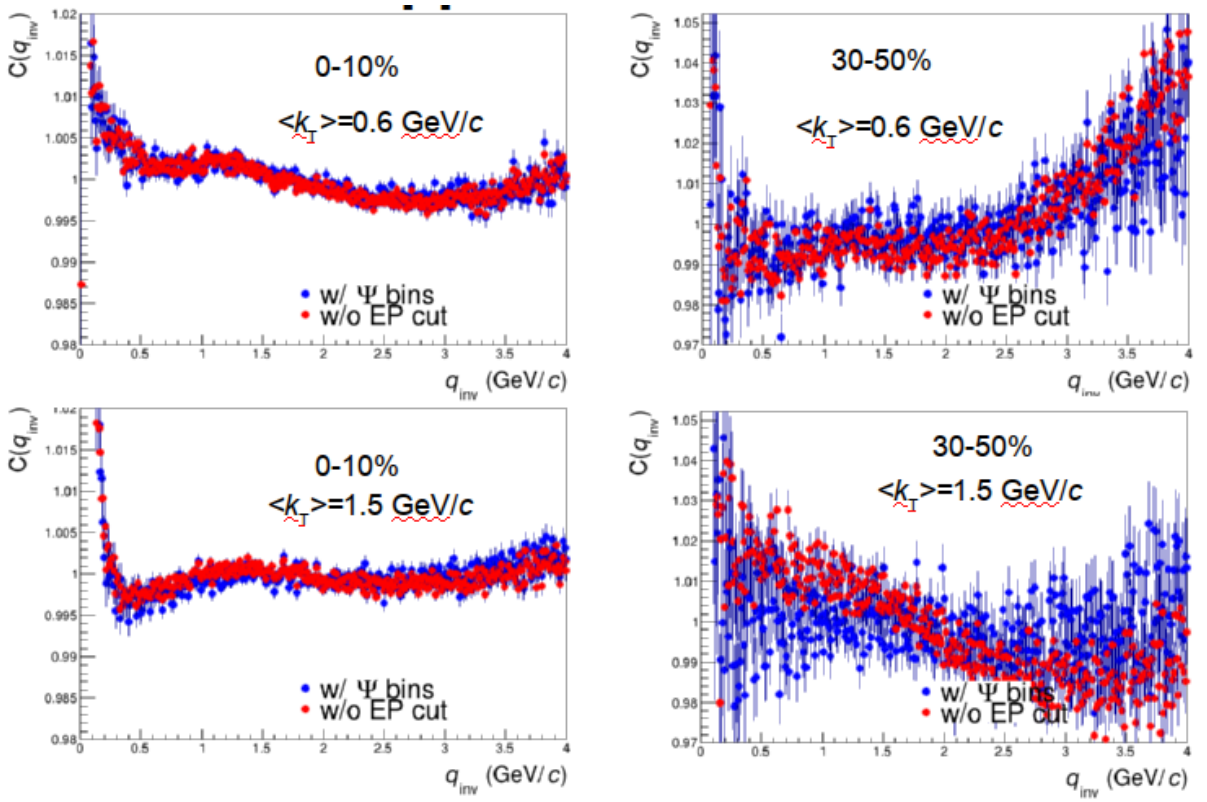

Fig. 14: Comparison of antiproton-antiproton correlation functions calculated without and with 6 event plane angle selection.

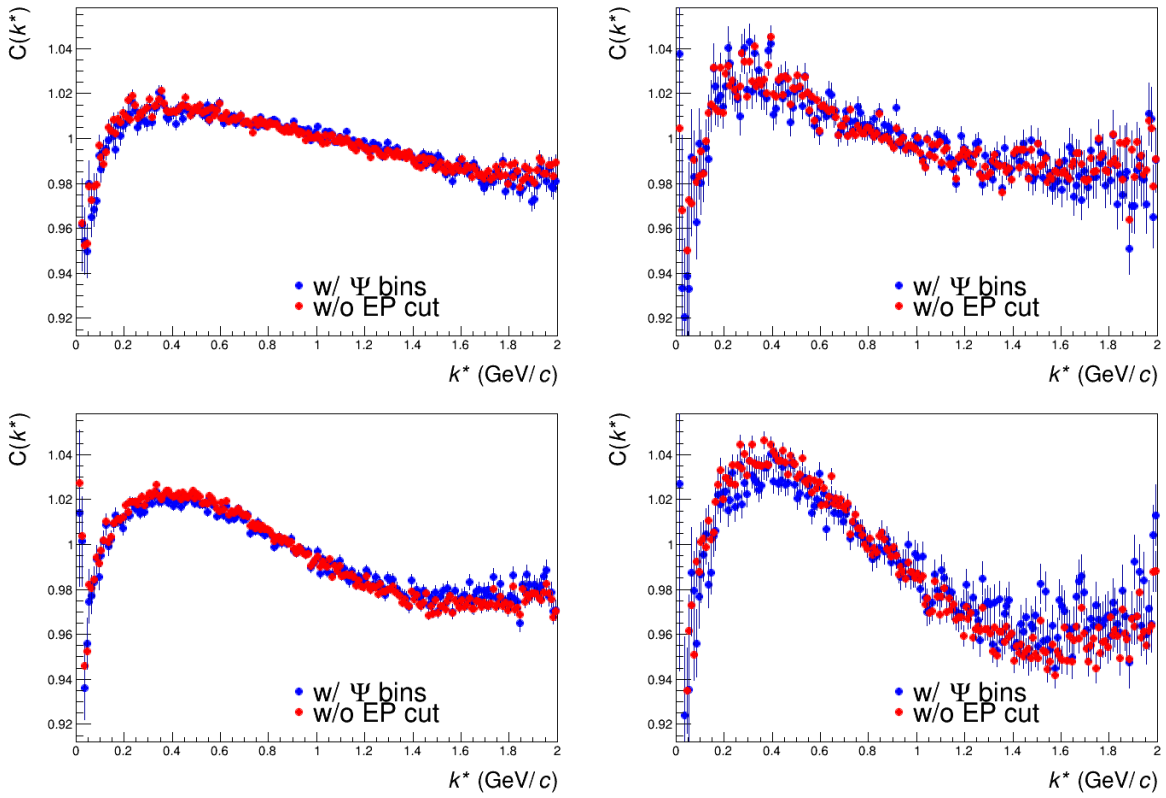

Fig. 15: Comparison of proton-antiproton of correlation functions calculated without and with 3 event plane angle selection. Top plots: $\langle k_T \rangle = 0.6 GeV/c$, bottom plots: $\langle k_T \rangle = 1.5 GeV/c$, left plots: $10-30\%$, right plots: $30-50\%$

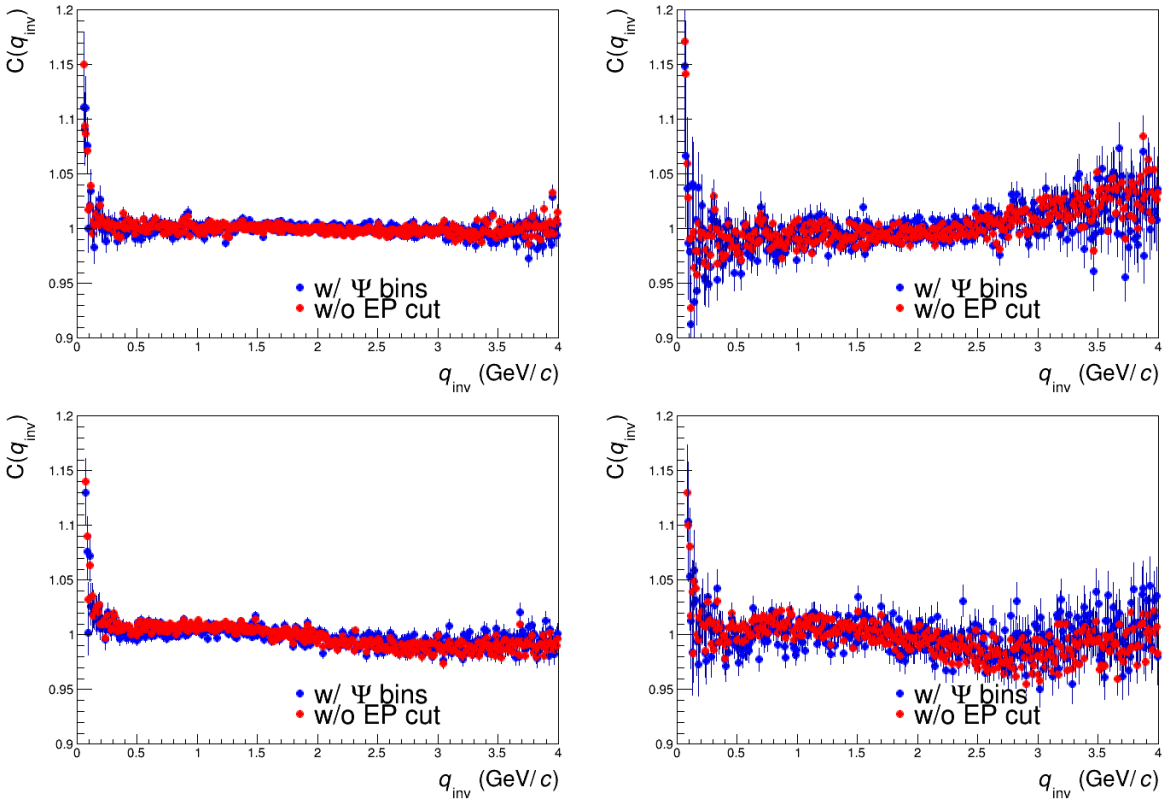

Fig. 16: Comparison of proton-proton of correlation functions calculated without and with 3 event plane angle selection. Top plots: $\langle k_T \rangle = 0.6 GeV/c$, bottom plots: $\langle k_T \rangle = 1.5 GeV/c$, left plots: $10-30\%$, right plots: $30-50\%$

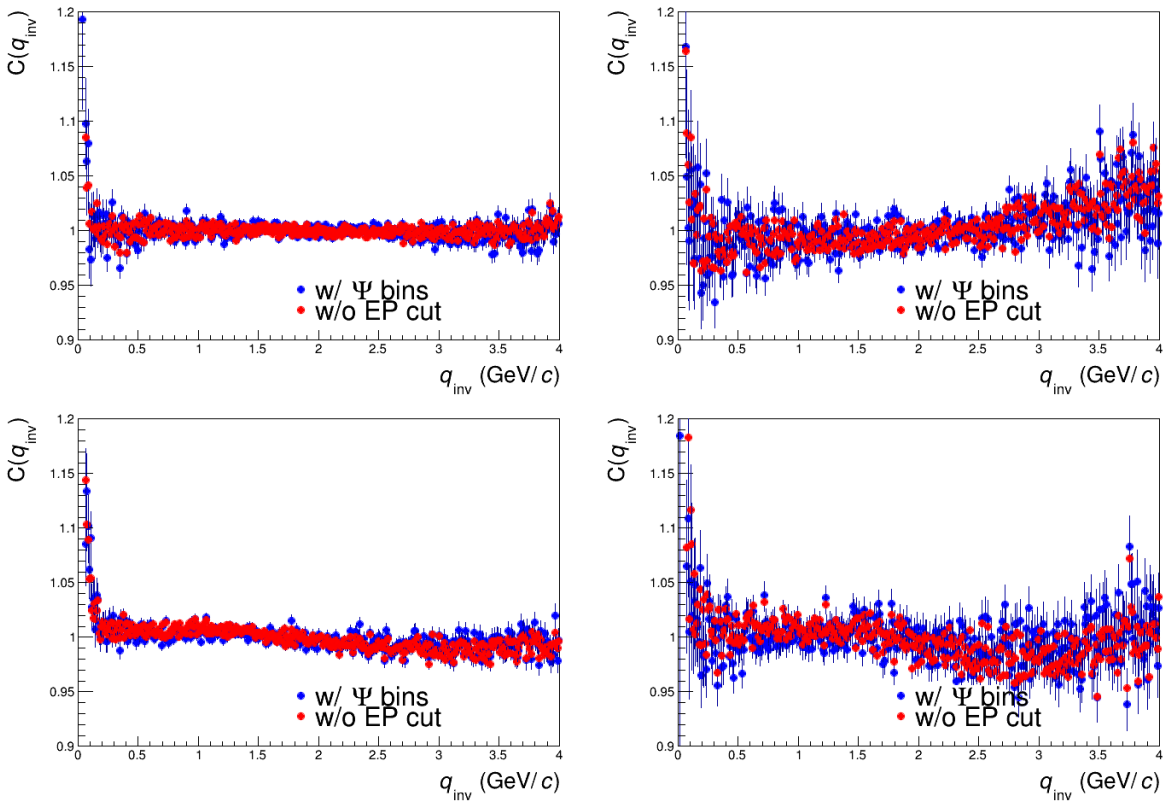

Fig. 17: Comparison of antiproton-antiproton of correlation functions calculated without and with 3 event plane angle selection. Top plots: $\langle k_T \rangle = 0.6 GeV/c$, bottom plots: $\langle k_T \rangle = 1.5 GeV/c$, left plots: $10-30\%$, right plots: $30-50\%$

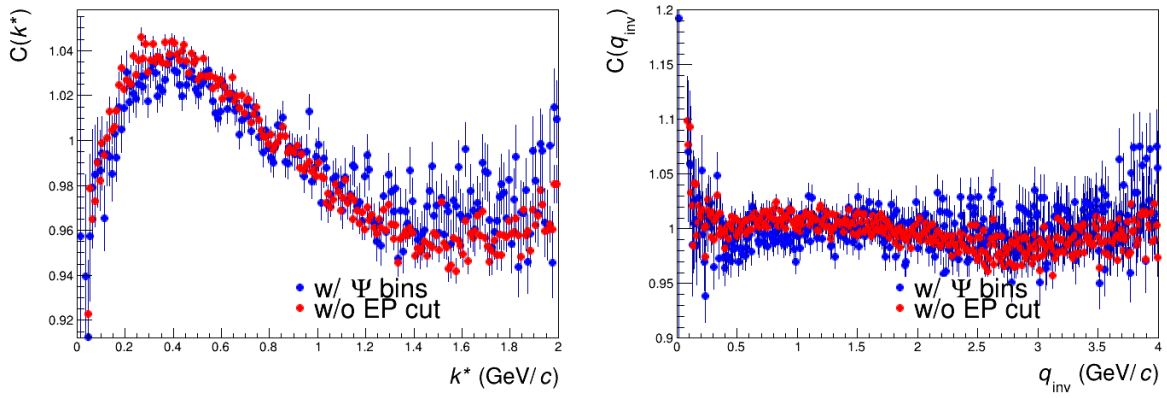

Fig. 18: Comparison of proton-antiproton (left plot) and proton-proton (right plot) correlation functions calculated without and with 12 event plane angle selection ($\langle k_T \rangle = 1.5 GeV/c$, centrality$30-50\%$

)

Due to high memory cost of the method with binning in event plane angle, all subsequent results were obtained using standard method, without event plane angle selection. It is justified as there are no significant differences on the low-q region, which contains femtoscopic information and plays a key role in fitting.

3.2 Correlation functions

Correlation functions were calculated with different sets of cuts which are summarized in Tab. 2

	$p_T(GeV/c)$	$DCA_{xy}(cm)$	$DCA_z(cm)$	PID	$\Delta\eta\Delta\varphi*$
set 1	0.7-4.0	2.4	3.2	3σ	–
set 2	0.7-4.0	2.4	3.2	3σ	$\lvert\Delta\eta\rvert < 0.01 \lvert\Delta\varphi*_{@R=1.2m}\rvert < 0.045$
set 3	0.7-4.0	**1.0**	3.2	3σ	$\lvert\Delta\eta\rvert < 0.01 \lvert\Delta\varphi*_{@R=1.2m}\rvert < 0.045$
set 4	0.7-4.0	2.4	3.2	$\mathbf{2\sigma}$	$\lvert\Delta\eta\rvert < 0.01 \lvert\Delta\varphi*_{@R=1.2m}\rvert < 0.045$
set 5	**0.3-5.0**	2.4	3.2	3σ	$\lvert\Delta\eta\rvert < 0.01 \lvert\Delta\varphi*_{@R=1.2m}\rvert < 0.045$

Table 2: The summary of cuts used in the analysis.

3.2.1 Influence of two-track cut

In Fig. 19, the comparison of pp, $\bar{\text{p}}\bar{\text{p}}$ and $\text{p}\bar{\text{p}}$ correlation functions with and without the cut on angular distance is presented. The cut strongly affects correlation functions of identical pairs and is important to limit splitting and mergin effects. On the other hand, the cut does not influence proton-antiproton correlations as there are no such pairs in the cut region.

3.2.2 Influence of DCA cut value

In Fig. 20, the comparison of pp, $\bar{\text{p}}\bar{\text{p}}$ and $\text{p}\bar{\text{p}}$ correlation functions with different cut on distance of closest approach in the transverse plane (2.4 cm vs. 1.0 cm) is presented. Results suggest that such a difference in track selection does not influnce two-particle correlations. Therefore, we choose 2.4 cm cut to have better statistics.

3.2.3 Influence of PID selection

In Fig. 21, the comparison of pp, $\bar{\text{p}}\bar{\text{p}}$ and $\text{p}\bar{\text{p}}$ correlation functions with different PID selection (3σ vs. 2σ cut) is presented. Results suggest that such a difference in PID selection does not influnce two-particle correlations. Therefore, we choose 3σ cut to have better statistics.

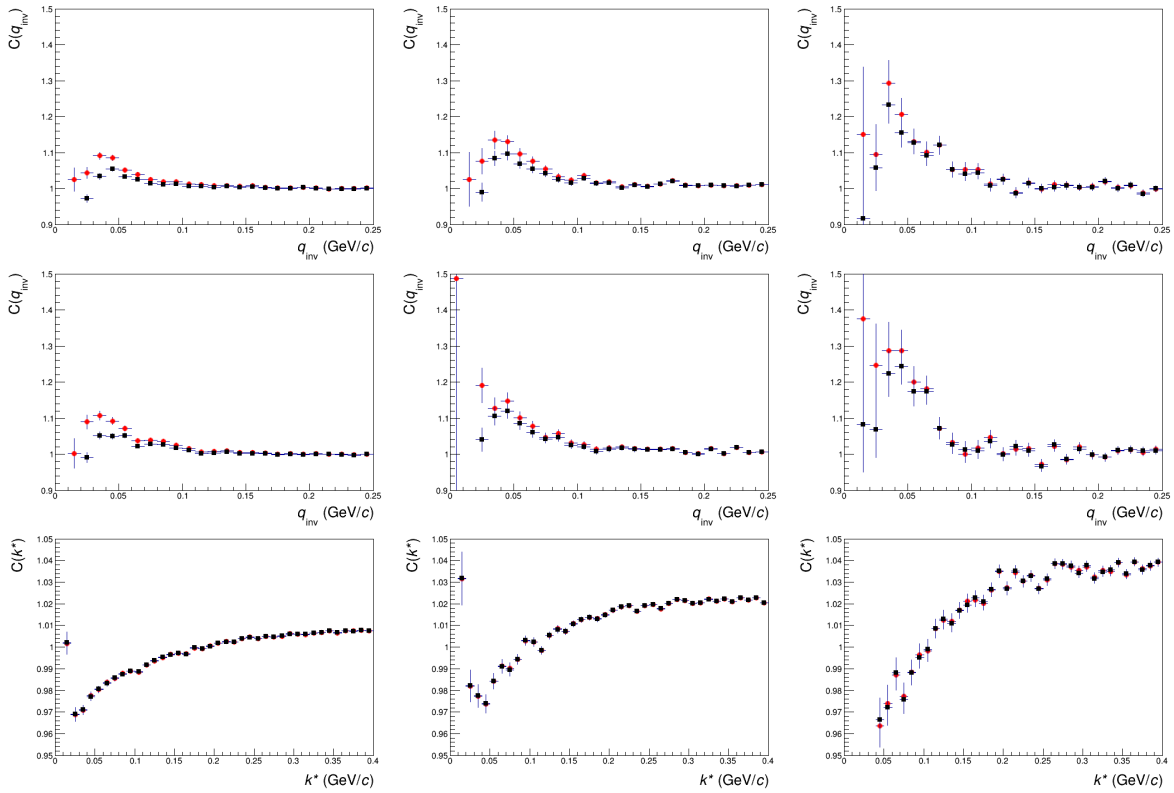

Fig. 19: Influnce of two-track cut: $|\Delta\eta| < 0.01 | \Delta\varphi *_{@R=1.2m} | < 0.045$ in red, no cut in black. Top row: proton-proton correlation functions for the $\sqrt{s_{\rm NN}} = 2.76$ TeV Pb–Pb collision data. Middle row: antiproton-antiproton correlation functions for the $\sqrt{s_{\rm NN}} = 2.76$ TeV Pb–Pb collision data. Bottom row: proton-antiproton correlation functions for the $\sqrt{s_{\rm NN}} = 2.76$ TeV Pb–Pb collision data. Results are shown for 0-10 %, 10-30 %, 30-50 % from left to right and $0.01 < k_{\rm T} < 5$ GeV/c.

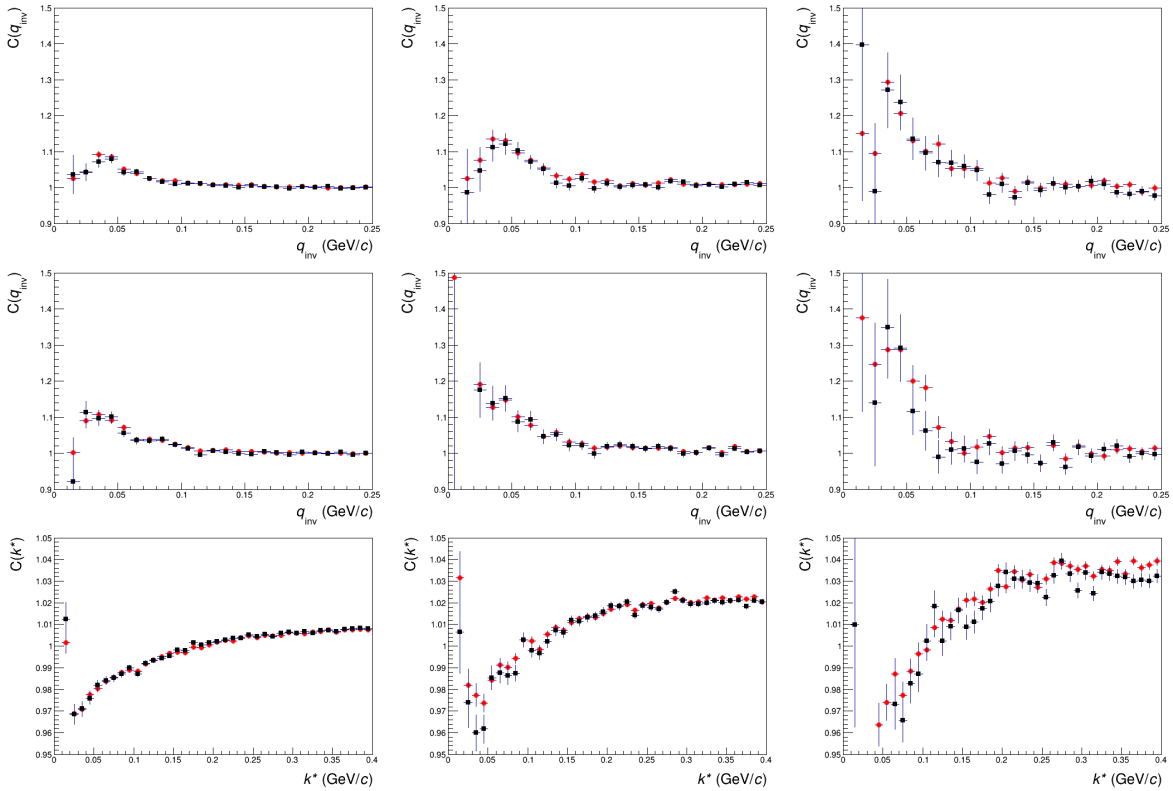

Fig. 20: Influence of DCA: cut 2.4 cm in red, cut 1.0 cm in black. Top row: proton-proton correlation functions for the $\sqrt{s_{\rm NN}} = 2.76$ TeV Pb–Pb collision data. Middle row: antiproton-antiproton correlation functions for the $\sqrt{s_{\rm NN}} = 2.76$ TeV Pb–Pb collision data. Bottom row: proton-antiproton correlation functions for the $\sqrt{s_{\rm NN}} = 2.76$ TeV Pb–Pb collision data. Results are shown for 0-10 %, 10-30 %, 30-50 % from left to right and $0.01 < k_{\rm T} < 5$ GeV/c.

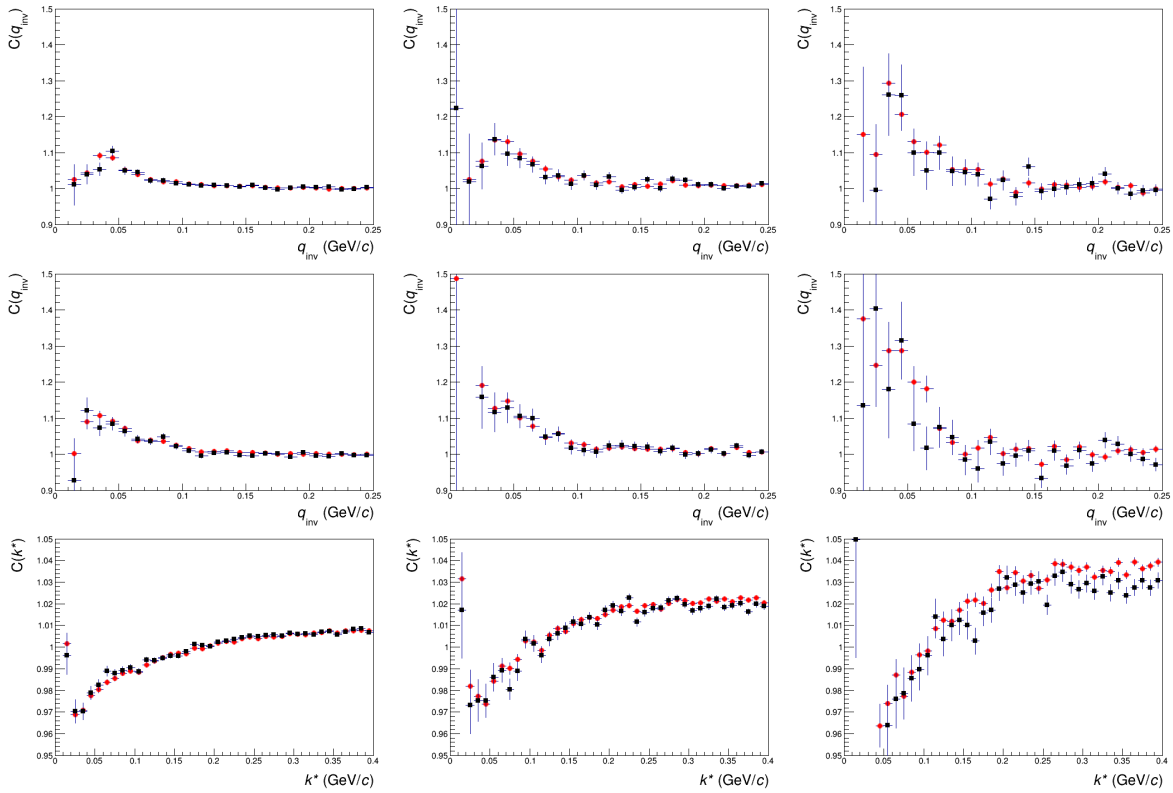

Fig. 21: Influence of PID: 3σ cut in red, 2σ cut in black. Top row: proton-proton correlation functions for the $\sqrt{s_{\mathrm{NN}}} = 2.76$ TeV Pb–Pb collision data. Middle row: antiproton-antiproton correlation functions for the $\sqrt{s_{\mathrm{NN}}} = 2.76$ TeV Pb–Pb collision data. Bottom row: proton-antiproton correlation functions for the $\sqrt{s_{\mathrm{NN}}} = 2.76$ TeV Pb–Pb collision data. Results are shown for 0-10 %, 10-30 %, 30-50 % from left to right and $0.01 < k_{\mathrm{T}} < 5$ GeV/c.

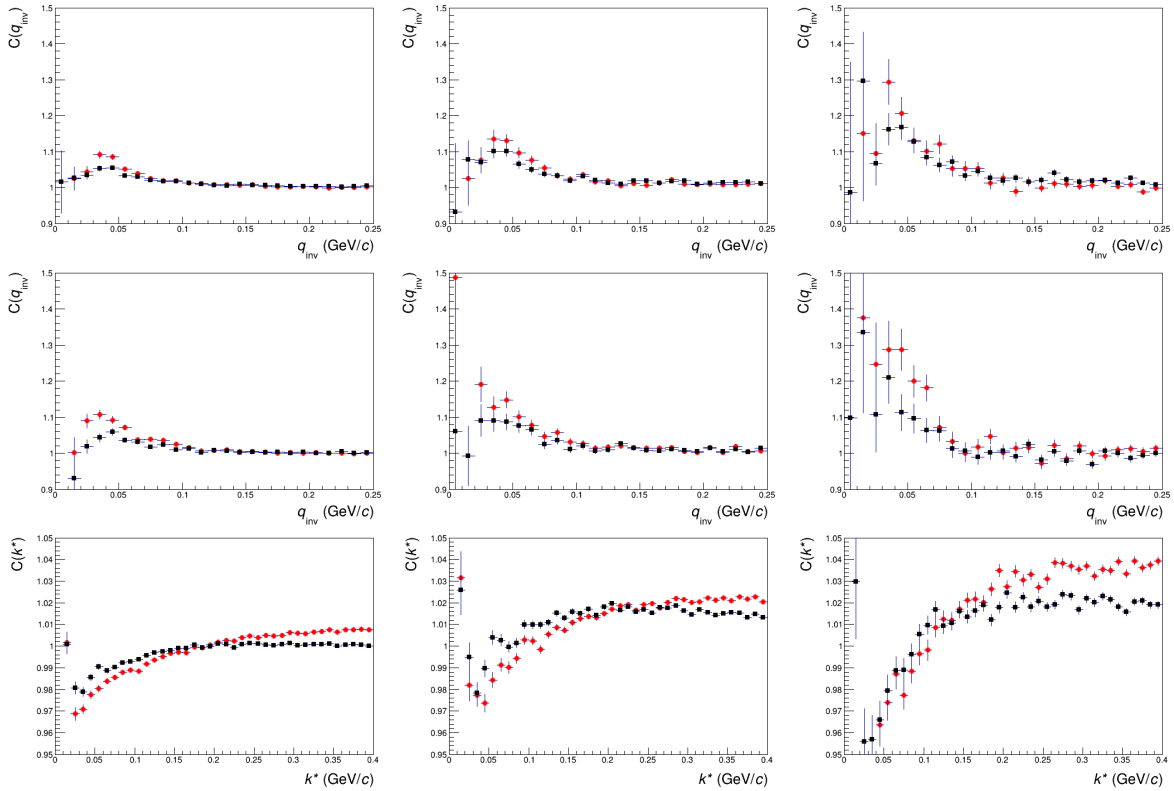

Fig. 22: Influence of p_T selection: $0.7 < p_T < 4.0 GeV/c$ in red, $0.3 < p_T < 5.0 GeV/c$ in black. Top row: proton-proton correlation functions for the $\sqrt{s_{\rm NN}} = 2.76$ TeV Pb–Pb collision data. Middle row: antiproton-antiproton correlation functions for the $\sqrt{s_{\rm NN}} = 2.76$ TeV Pb–Pb collision data. Bottom row: proton-antiproton correlation functions for the $\sqrt{s_{\rm NN}} = 2.76$ TeV Pb–Pb collision data. Results are shown for 0-10 %, 10-30 %, 30-50 % from left to right and $0.01 < k_{\rm T} < 5$ GeV/c.

3.2.4 Influence of p_T selection

In Fig. 22, the comparison of pp, $\bar{\rm p}\bar{\rm p}$ and $\rm p\bar{p}$ correlation functions with different p_T selection ($0.7-4.0$GeV/c vs. $0.3-5.0$GeV/c) is presented. Plots indicate that this cut influences results significantly. It might be caused by (anti)protons with small transverse momentum, coming from weak decays and from interactions with material of the detector. To reduce this effect, we choose p_T region $0.7-4.0$ GeV/c.

In Fig. 23, 24, 25 and 26 the correlation functions of pp, $\bar{\rm p}\bar{\rm p}$ and $\rm p\bar{p}$ systems are presented.

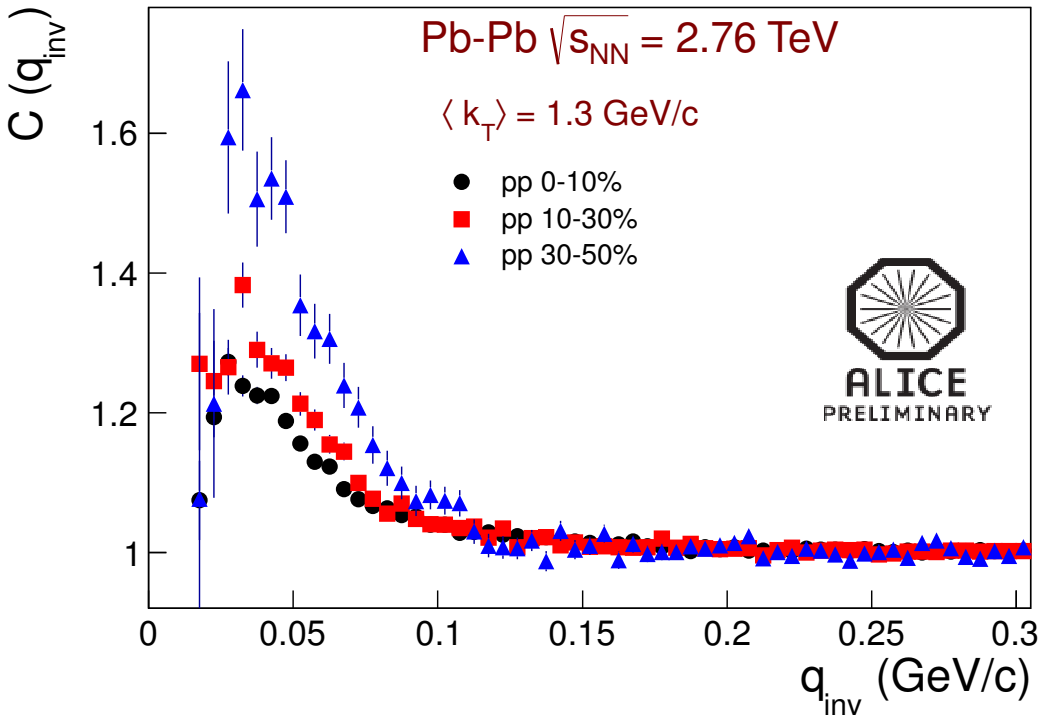

Fig. 23: Proton-proton correlation functions for the $\sqrt{s_{\rm NN}} = 2.76$ TeV Pb–Pb collision data.

In case of identical systems, the expected maximum due to strong interactions for $q_{\rm inv} \approx 40$ MeV/c is clearly visible. The results reveal that proton-proton and antiproton-antiproton correlations are consistent. Also, the centrality dependence is understandable - the more peripheral the events, the stronger the correlation effect is. It means that the size of the emitting source is growing with multiplicity. Proton-antiproton correlations show expected behaviour - a maximum for the lowest momentum difference due to Coulomb attraction, then a minimum caused by the annihilation processes. Another observed feature is the flat background of the correlation function at large values of momentum difference which indicates the absence of wide non-femtoscopic structures.

In Fig. 27 the correlation functions are compared with those calculated without the cut on angular distance. Differences in correlation functions are within statistical errors.

In Fig. 28 the comparison of correlation functions calculated for "field $--$" and "field $++$" runs is shown. The only visible difference can be noticed for proton-antiproton correlation function (centrality $0-10\%$). However, radii fitted for these functions are within statistical and systematic errors shown below.

Fitting the correlation functions for proton systems can be performed with the software package `CorrFit`. However, as it can be seen in Fig. 29, attempts to fit the obtained correlation functions directly with `CorrFit` failed. Correlation of pp pairs has three components. The Coulomb and quantum statistics have to be negative (e.g. give the correlation function below unity). The strong interaction is positive but has limited width - one can think of it as a resonance peak. Therefore, the excess in the range $30-80$ MeV/c of k^* cannot be explained by correlations coming from the pp wave function. A significant influence of residual correlations may be a possible explanation. As the influence of residual correlations seems to be significant, the method of simultaneous fitting of pp ($\bar{\rm p}\bar{\rm p}$) and pΛ ($\bar{\rm p}\bar{\Lambda}$) correlations was proposed. It is assumed that residual correlations coming from pΣ^+ system are negligible, due to a known small cross-section for this system. Hence, the experimental correlation function of pp and $\bar{\rm p}\bar{\rm p}$ systems were

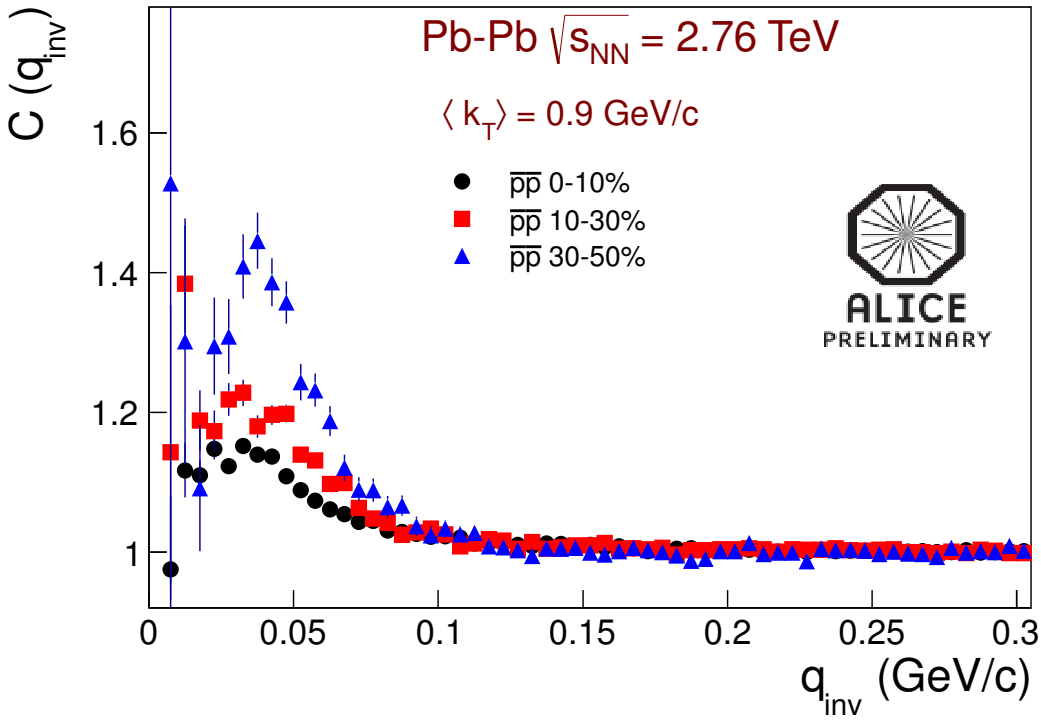

Fig. 24: Antiproton-antiproton correlation functions for the $\sqrt{s_{\rm NN}} = 2.76$ TeV Pb–Pb collision data ($\langle k_{\rm T} \rangle = 0.9$ GeV/c).

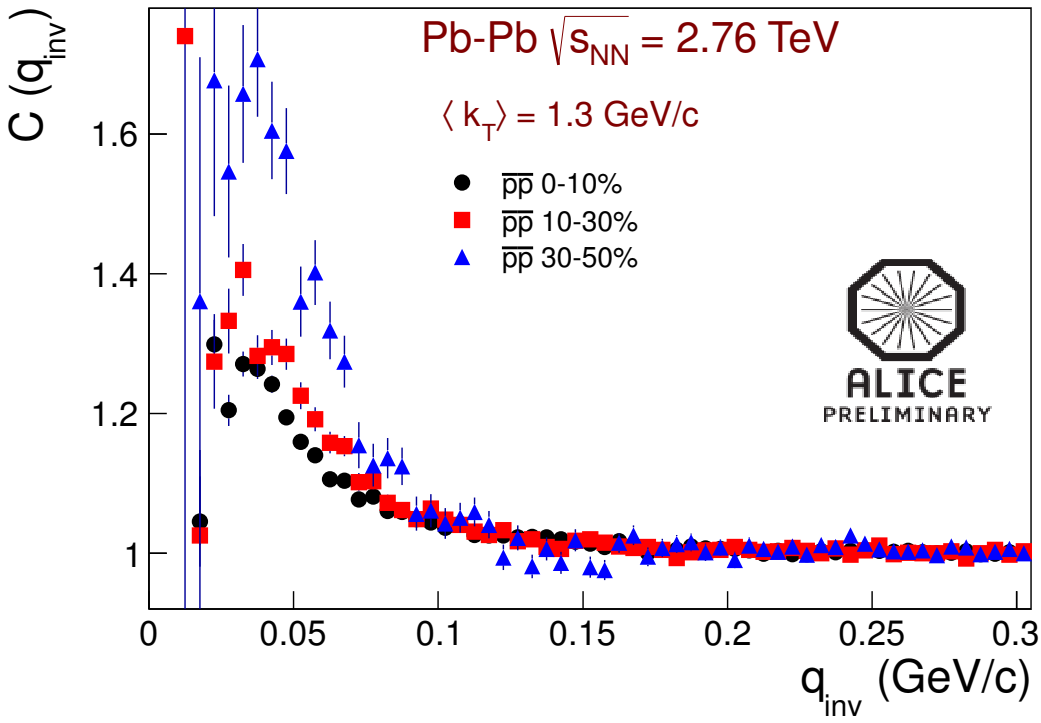

Fig. 25: Antiproton-antiproton correlation functions for the $\sqrt{s_{\rm NN}} = 2.76$ TeV Pb–Pb collision data ($\langle k_{\rm T} \rangle = 1.3$ GeV/c).

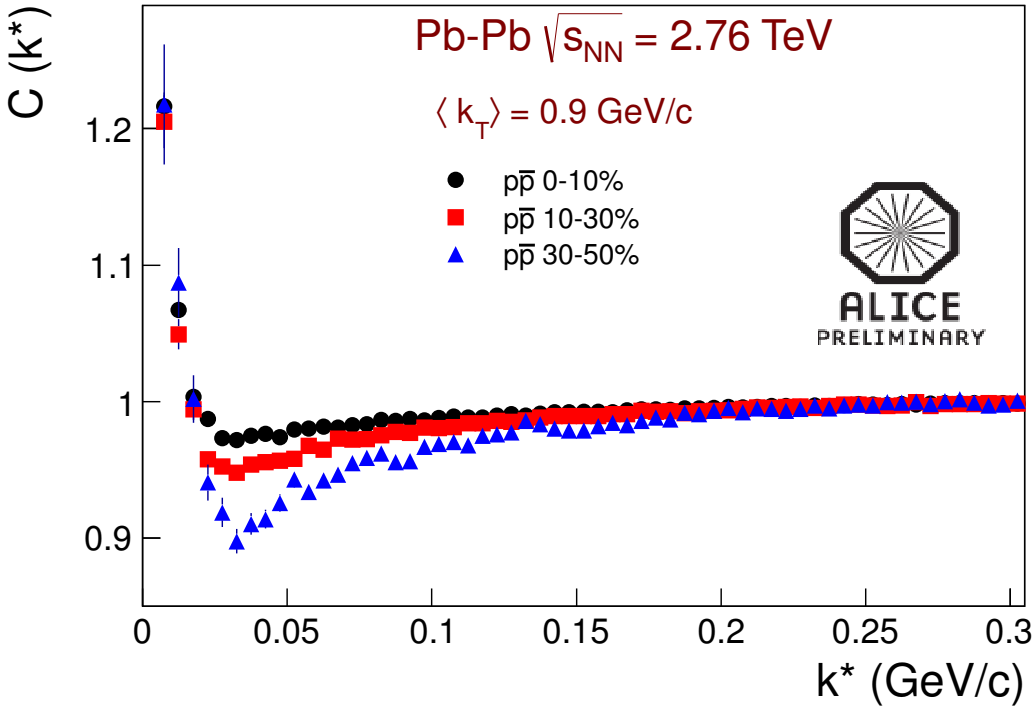

Fig. 26: Proton-antiproton correlation functions for the $\sqrt{s_{\rm NN}} = 2.76$ TeV Pb–Pb collision data.

fitted with the formula:

$$C_{\rm meas}(k^*_{\rm pp}) = 1 + \lambda_{\rm pp} \cdot (C_{\rm pp}(k^*_{\rm pp};R) - 1) + \lambda_{\rm p\Lambda} \cdot (C_{\rm p\Lambda}(k^*_{\rm pp};R) - 1), \quad (2)$$

where:

- $\lambda_{\rm pp}$, $\lambda_{\rm p\Lambda}$ - parameters which describes the relative number of pp pairs where both particles are primary ($\lambda_{\rm pp}$) and pairs where one particle is primary, the other is a product of Λ decay ($\lambda_{\rm p\Lambda}$),
- R - radius
- $C_{\rm pp}(k^*_{\rm pp};R)$ - theoretical proton-proton correlation function for given R (Gaussian source assumed), obtained from `CorrFit`,
- $C_{\rm p\Lambda}(k^*_{\rm pp};R) = \sum_{k^*_{\rm p\Lambda}} C_{\rm p\Lambda}(k^*_{\rm p\Lambda}) T(k^*_{\rm pp}, k^*_{\rm p\Lambda})$ - theoretical pΛ correlation function for given R obtained from Lednicky's model,
- $T(k^*_{\rm pp}, k^*_{\rm p\Lambda})$ - transformation factors related to Λ decay kinematics, calculated with `THERMINATOR`.

The pΛ correlation function obtained with Lednicky's model is calculated as a function of $k^*_{\rm p\Lambda}$, but according to Eq. (2), there is a need to use $C_{\rm p\Lambda}$ dependent on the relative momentum between two protons. Therefore, relevant transformation should be performed, namely for each value of $k^*_{\rm pp}$, $C_{\rm p\Lambda}$ is determined as a sum over all $k^*_{\rm p\Lambda}$ values of $C_{\rm p\Lambda}$ obtained with Lednicky's model scaled by factors from the two-dimensional histogram $T(k^*_{\rm pp}, k^*_{\rm p\Lambda})$ calculated with `THERMINATOR`:

$$C_{\rm p\Lambda}(k^*_{\rm pp};R) = \sum_{k^*_{\rm p\Lambda}} C_{\rm p\Lambda}(k^*_{\rm p\Lambda}) T(k^*_{\rm pp}, k^*_{\rm p\Lambda}). \quad (3)$$

The kinematics dependence of Λ decay $T(k^*_{\rm pp}, k^*_{\rm p\Lambda})$ is shown in Fig. 30. Fig. 31 shows an example of the transformation of $C_{\rm p\Lambda}$.

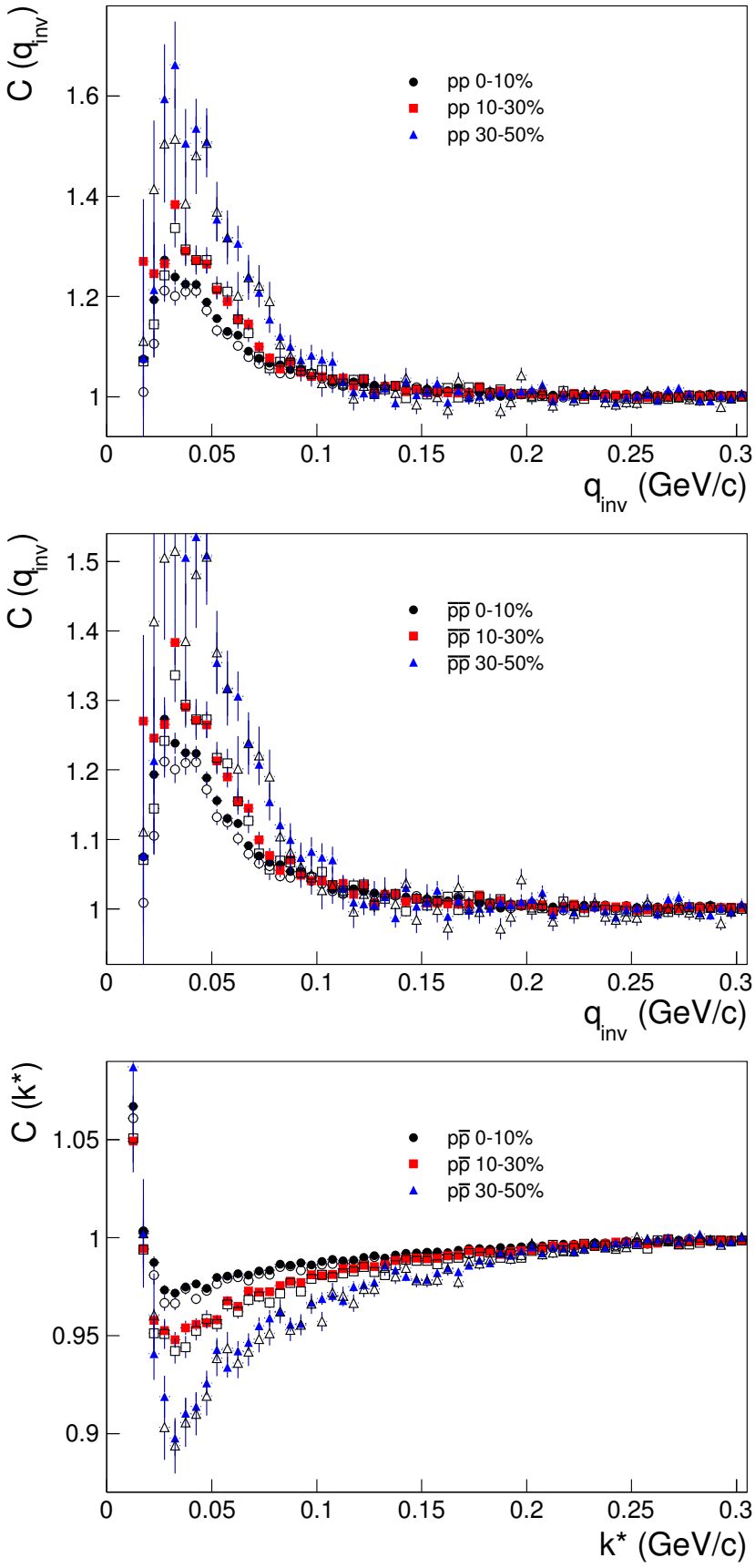

Fig. 27: From top to bottom: proton-proton, antiproton-antiproton and proton-antiproton correlation functions. Results before (open markers) and after (solid markers) applying the cut on angular distance are shown.

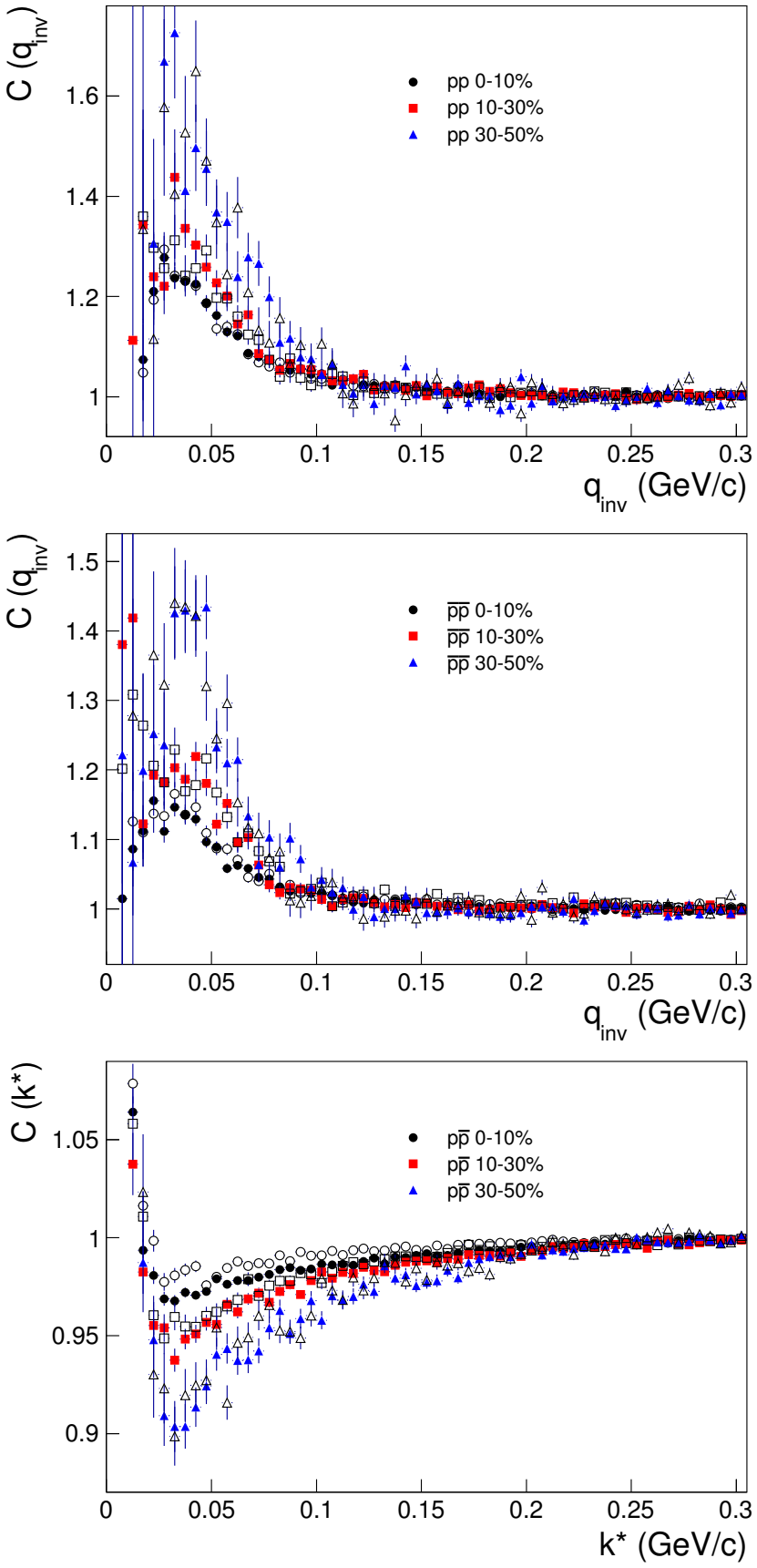

Fig. 28: From top to bottom: proton-proton, antiproton-antiproton and proton-antiproton correlation functions. Results for "field ++" runs (open markers) and "field −−" runs (solid markers) are shown.

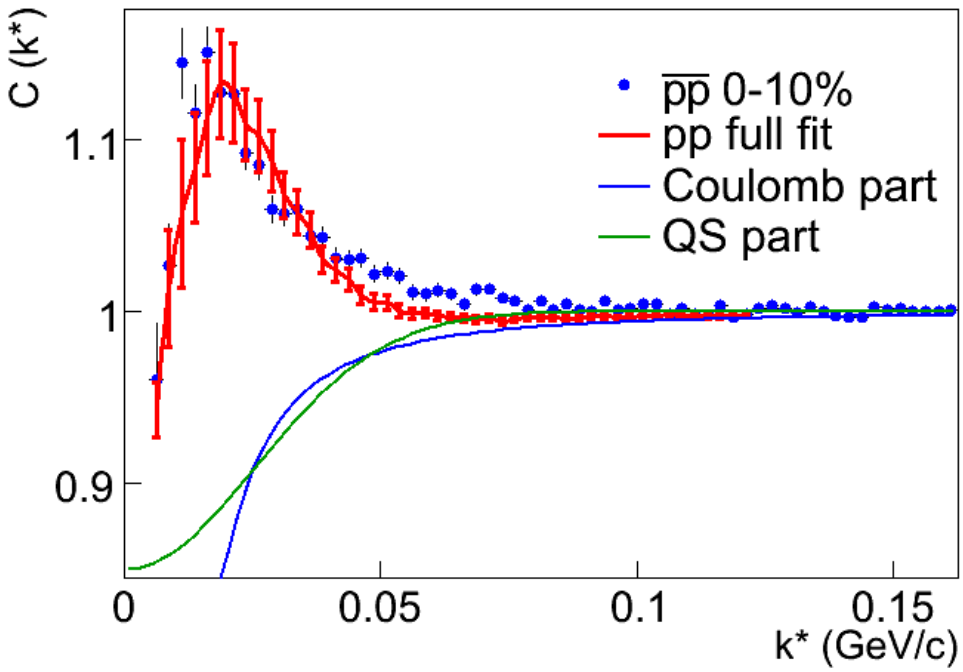

Fig. 29: Comparison of experimental correlation functions and fit obtained with `CorrFit` [4]. Contribution of Coulomb repulsion and Quantum Statistics are also shown [5].

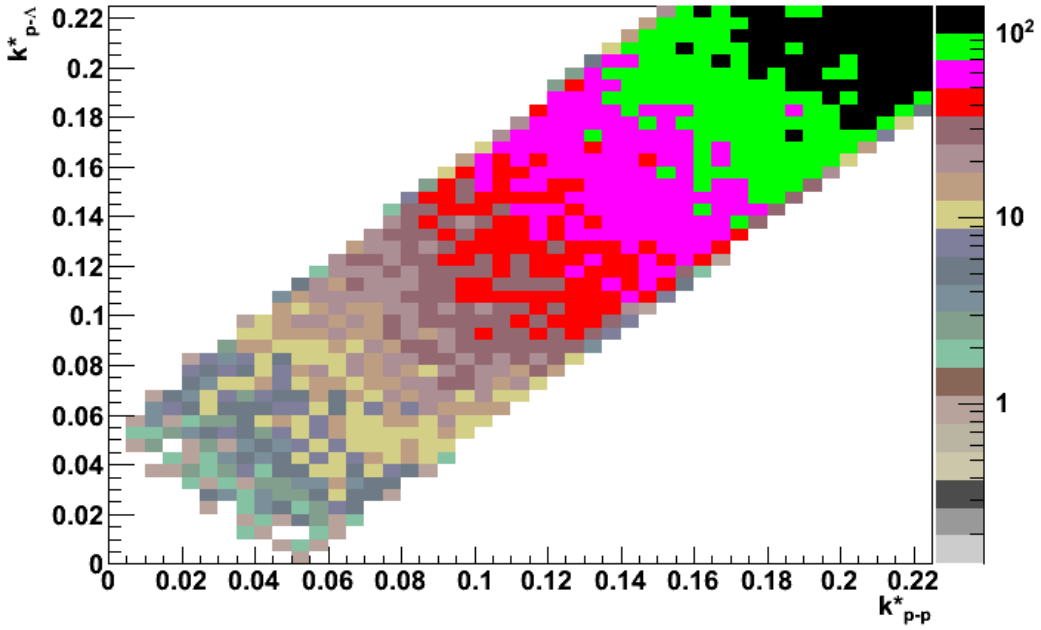

Fig. 30: Kinematics dependence of Λ decay $T(k^*_{\mathrm{pp}}, k^*_{\mathrm{p}\Lambda})$ calculated with `THERMINATOR`.

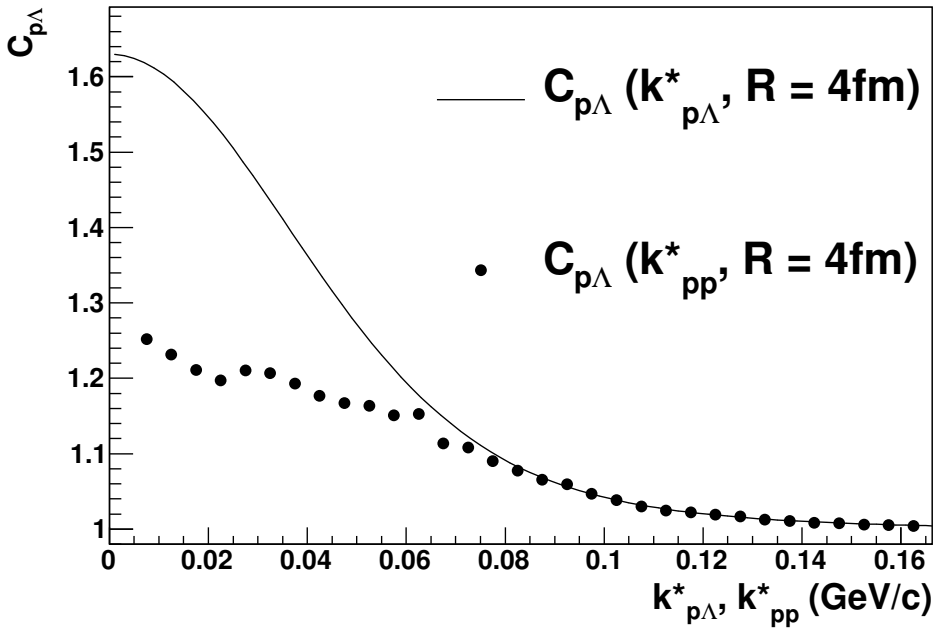

Fig. 31: Example of the transformation of $C_{\mathrm{p}\Lambda}(k^*_{\mathrm{p}\Lambda}) \rightarrow C_{\mathrm{p}\Lambda}(k^*_{\mathrm{pp}})$.

As far as fitting the $\mathrm{p}\bar{\mathrm{p}}$ correlations are concerned, the relevant formula is analogous to Eq. (2) and takes the following form:

$$C_{\mathrm{meas}}(k^*_{\mathrm{p}\bar{\mathrm{p}}}) = 1 + \lambda_{\mathrm{p}\bar{\mathrm{p}}} \cdot (C_{\mathrm{p}\bar{\mathrm{p}}}(k^*_{\mathrm{p}\bar{\mathrm{p}}}; R) - 1) + \lambda_{\bar{\mathrm{p}}\Lambda} \cdot (C_{\bar{\mathrm{p}}\Lambda}(k^*_{\mathrm{p}\bar{\mathrm{p}}}; R) - 1). \quad (4)$$

The $\bar{\mathrm{p}}\Lambda$ correlation function calculated with the analytical model of Lednicky and Lyuboshitz and its form after the transformation to the reference frame of two protons (one of which comes from Λ decay) are shown in Fig. 32.

pp ($\mathrm{p}\bar{\mathrm{p}}$) and $\mathrm{p}\Lambda$ ($\bar{\mathrm{p}}\Lambda$) correlation functions have been calculated for the emission radii from 1.0 fm to 6.0 fm with a step of 0.1 fm. The fitting procedure is performed making use of MINUIT minimisation package. A gradient minimisation algorithm (MIGRAD) is used to find a minimum χ^2 value calculated between the experimental correlation function and the functions defined by Eq. (2) and (4) calculated for given parameters λ_{pp}, $\lambda_{\mathrm{p}\Lambda}$ ($\lambda_{\mathrm{p}\bar{\mathrm{p}}}$, $\lambda_{\bar{\mathrm{p}}\Lambda}$) and R by the quadratic interpolation of the theoretical correlation functions. It is assumed that the radii of pp ($\mathrm{p}\bar{\mathrm{p}}$) and $\mathrm{p}\Lambda$ ($\bar{\mathrm{p}}\Lambda$) sources are equal.

Fig. 33 and 34 are the examples of the fitting results for $\bar{\mathrm{p}}\bar{\mathrm{p}}$ and $\mathrm{p}\bar{\mathrm{p}}$ correlation functions. The fit qualitatively works, namely contribution from pp correlations describes the maximum at $k^* \approx 20$ MeV/c and wide correlations is reproduced by residual correlations coming from $\mathrm{p}\Lambda$ system.

We found following sources of the systematic errors:

- constraints on the λ_{pp}, $\lambda_{\mathrm{p}\Lambda}$ parameters
  - fixing the ratio $\lambda_{\mathrm{pp}}/\lambda_{\mathrm{p}\Lambda}$ to values estimated from the fits to pp, $\bar{\mathrm{p}}\bar{\mathrm{p}}$, $\mathrm{p}\bar{\mathrm{p}}$, setting the λ_{pp} and $\lambda_{\mathrm{p}\Lambda}$ paramters free, causes the maximum change of the radius 13% (usually $< 5\%$)
  - fixing to estimates from AMPT (see Tab.8): in general, fit fails, hence it is not considered in the systematics error,
- fitting procedure

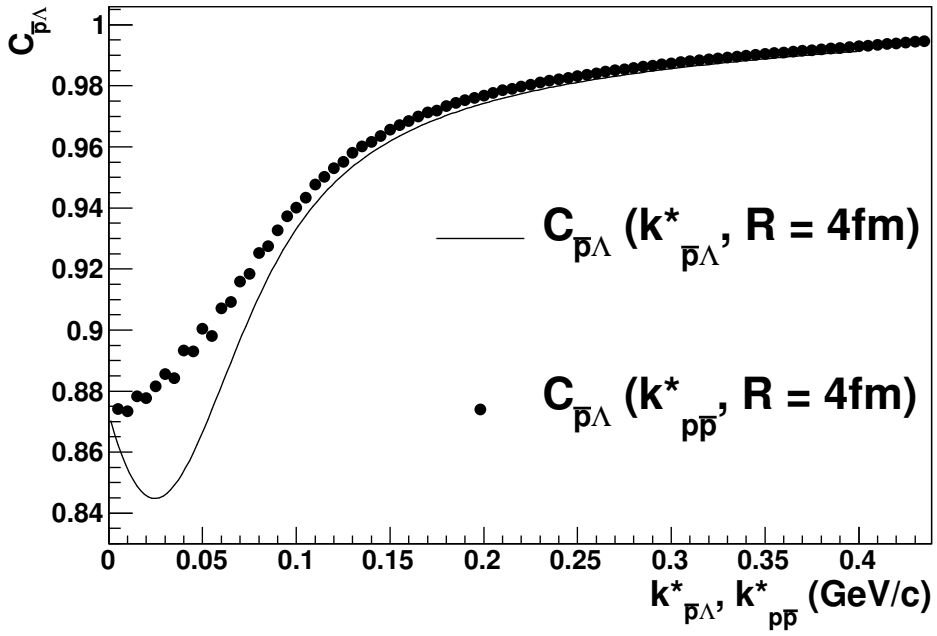

Fig. 32: The $\bar{p}\Lambda$ correlation function calculated with the analytical model of Lednicky and Lyuboshitz and its form after the transformation: $C_{\bar{p}\Lambda}(k^*_{\bar{p}\Lambda}) \rightarrow C_{\bar{p}\Lambda}(k^*_{p\bar{p}})$.

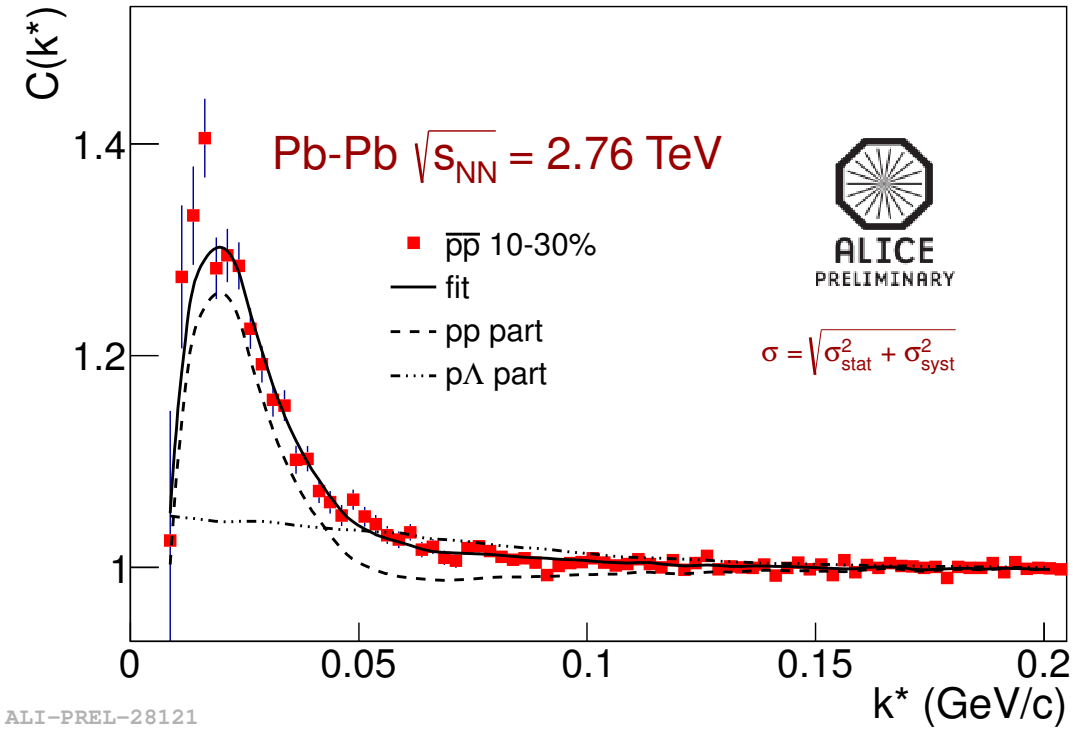

Fig. 33: Results of the fitting the $\bar{p}\bar{p}$ correlation function. The contribution of the theoretical pp and pΛ correlation functions scaled by factors related to the relevant fractions of pp pairs are shown with dashed and dotted-dashed lines, respectively.

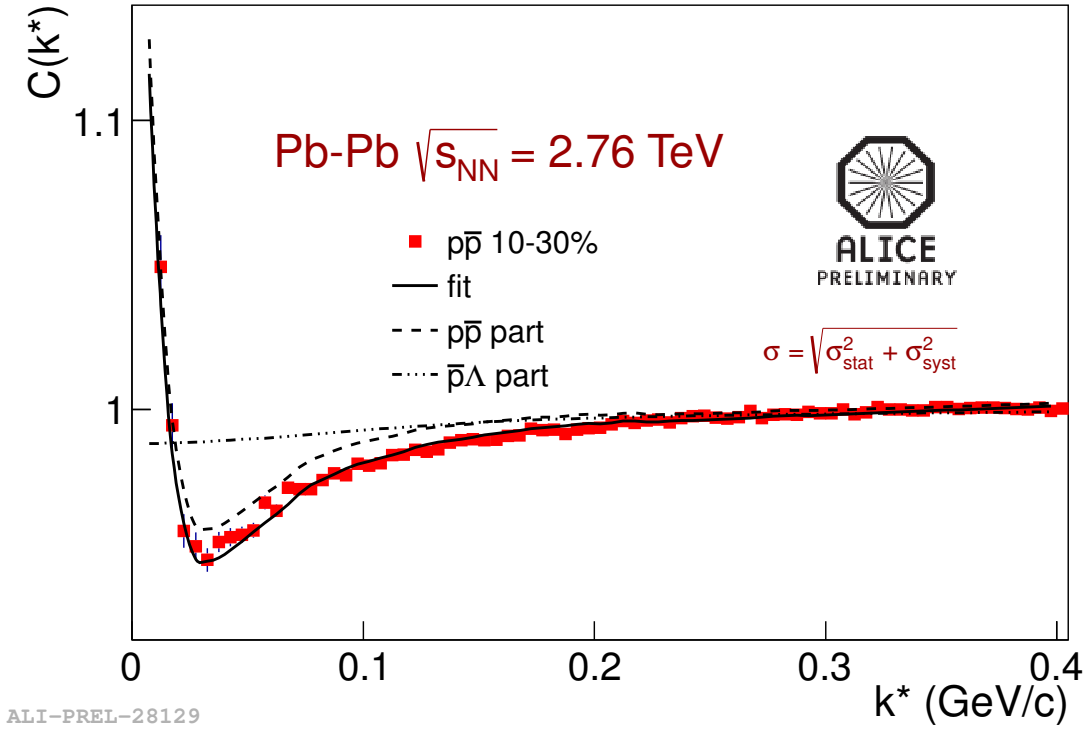

Fig. 34: Results of the fitting the pp̄ correlation function. The contributions of the theoretical pp̄ and p̄Λ correlation functions scaled by factors related to the relevant fractions of pp̄ pairs are shown with dashed and dotted-dashed lines, respectively.

- ranges of the fit and starting parameters - changing the fit range by $\pm 10\%$ causes the maximum change less than 6% for the radius (usually $< 2\%$); the fit is quite sensitive to significant changes of the starting paramters, but close to the minimum of the objective function, the change of the radius is negligible (however it is still under investigation)
- stability of the numerical fit - $< 10\%$ (usually $< 3\%$)

- assumption regarding $R_{p\Lambda}/R_{pp}$ ratio (following m_T scaling from hydrodynamics) - taking $R_{p\Lambda} = 0.95 R_{pp}$ causes the change of the radius less than 1%

- influence of the two track cuts (turning on and off the φ^* cut) - $< 10\%$ (usually $< 4\%$)

Systematic error for given system, centrality and k_T bin is estimated as the maximum error within each system. Maximum systematic error for the radius is estimated as: $+20\%$, -21%.

Tab. 3 contains the numerical values of the fitted radii with statistical and systematic errors. Fig. 35 shows the monotonic centrality dependence of the fitted radii for all combinations of pairs of (anti)protons.

	R (fm)			
	pp	p̄ p̄		pp̄
$\langle k_T \rangle$ (GeV/c)	1.3	0.9	1.3	0.9
0-10%	$3.15 \pm 0.05^{+0.63}_{-0.43}$	$3.41 \pm 0.05^{+0.44}_{-0.54}$	$3.14 \pm 0.04^{+0.28}_{-0.66}$	$3.47 \pm 0.05^{+0.23}_{-0.10}$
10-30%	$2.61 \pm 0.09^{+0.52}_{-0.37}$	$2.65 \pm 0.08^{+0.34}_{-0.42}$	$2.45 \pm 0.09^{+0.22}_{-0.51}$	$2.73 \pm 0.02^{+0.19}_{-0.08}$
30-50%	$2.34 \pm 0.14^{+0.46}_{-0.33}$	$2.50 \pm 0.01^{+0.33}_{-0.40}$	$2.50 \pm 0.01^{+0.23}_{-0.53}$	$2.69 \pm 0.02^{+0.19}_{-0.08}$

Table 3: Radii extracted from proton femtoscopy. Statistical and systematic errors are shown.

In Fig. 36 radii obtained in proton femtoscopy as well as those extracted from $\pi\pi$, $K^{\pm}K^{\pm}$ and $K^0_S K^0_S$ correlations are plotted versus $m_T = \sqrt{\langle k_T \rangle^2 + m_0^2}$. R_{inv} is scaled by the approximate kinematic factor

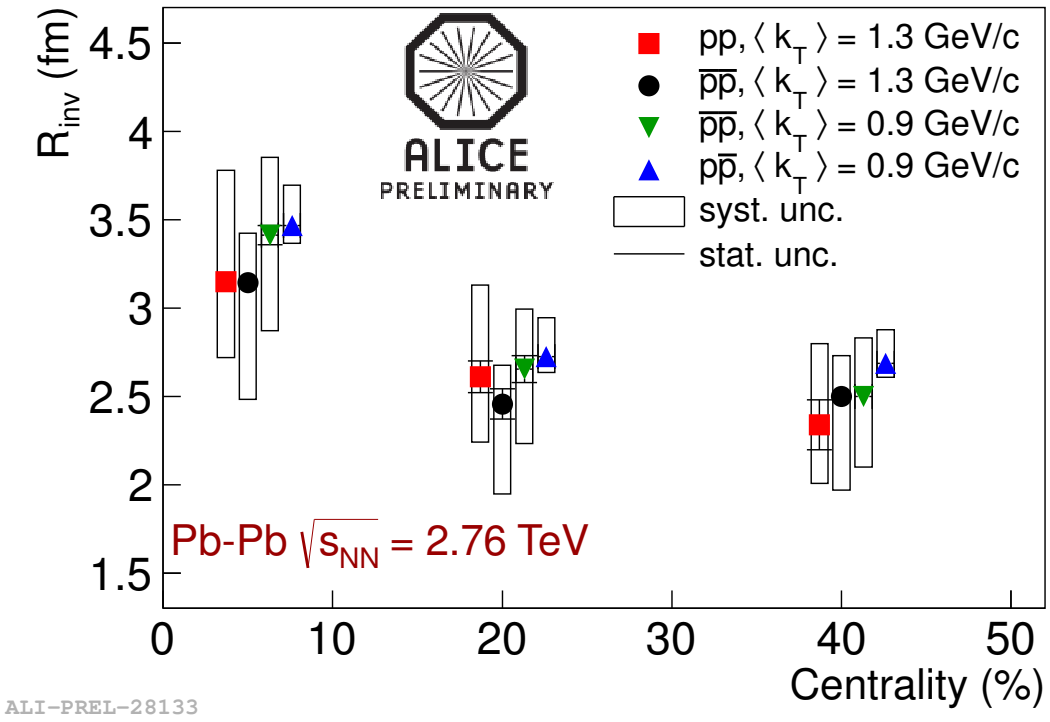

Fig. 35: Centrality dependence of the fitted radii from proton femtoscopy. Statistical (lines) and systematic (boxes) errors are shown.

$(\frac{\sqrt{\gamma}+2}{3})^{-1/2}$. Hydrodynamics predicts m_{T} of the radii calculated in LCMS (Longitudinally Co-Moving System). However, R_{inv} is calculated in PRF (Pair Rest Frame). Therefore, approximate m_{T} scaling may be recovered by using the given formula. In Fig. 37 results for charged and neutral kaons as well as for (anti)protons are combined using weighted mean method:

$$R_{\mathrm{mean}} = \frac{\sum_i R_i w_i}{\sum_i w_i}$$

$$SystErr_{\mathrm{mean}} = \frac{\sum_i SystErr_i w_i}{\sum_i w_i} + diff$$

$$w_i = \frac{1}{\sigma_i^2}$$

where σ_i - statistical error, $diff$ - the difference in radius between different pair types. Results for kaons are combined in the following way:

- 1.-4. m_{T} bins $K^{ch}K^{ch}$ + 1. m_{T} bin $K^0_S K^0_S$
- 5.-6. m_{T} bins $K^{ch}K^{ch}$ + 2. m_{T} bin $K^0_S K^0_S$
- 7. m_{T} bin $K^{ch}K^{ch}$ + 3. m_{T} bin $K^0_S K^0_S$
- 4. m_{T} bin $K^0_S K^0_S$

For protons, we combined the first m_{T} bins for pp̄ and p̄p̄ and the second m_{T} bins for pp and p̄p̄.

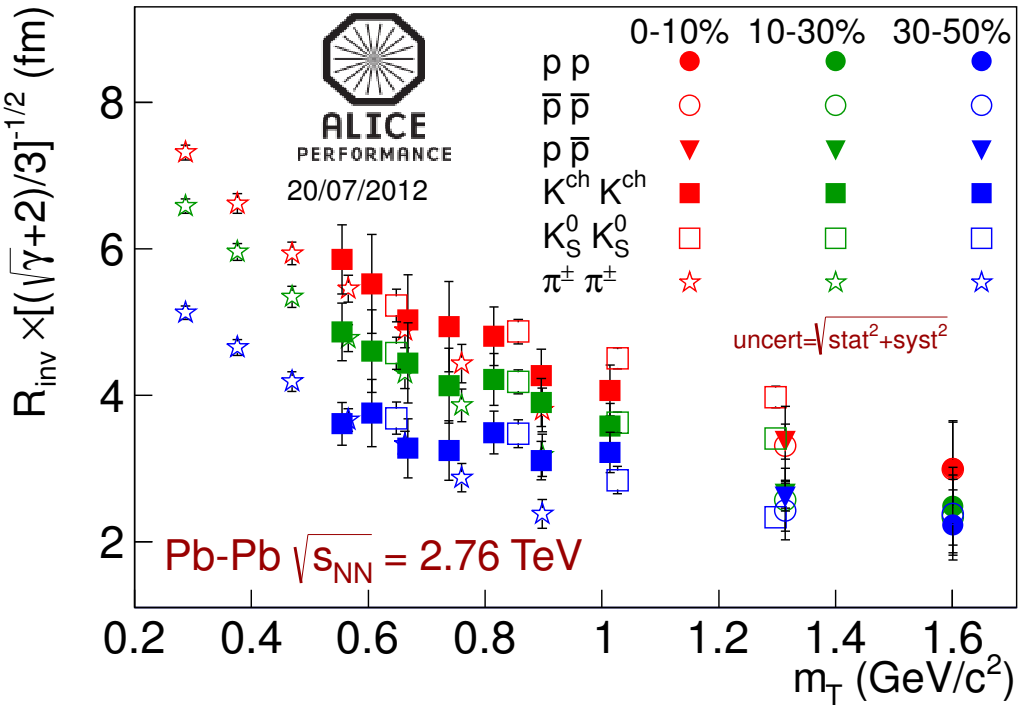

Fig. 36: m_{T} dependence of the radius parameter extracted from correlations of pions, charged kaons, neutral kaons and protons. Estimates of total errors (the quadrature sum of the statistical and the systematic ones) are shown.

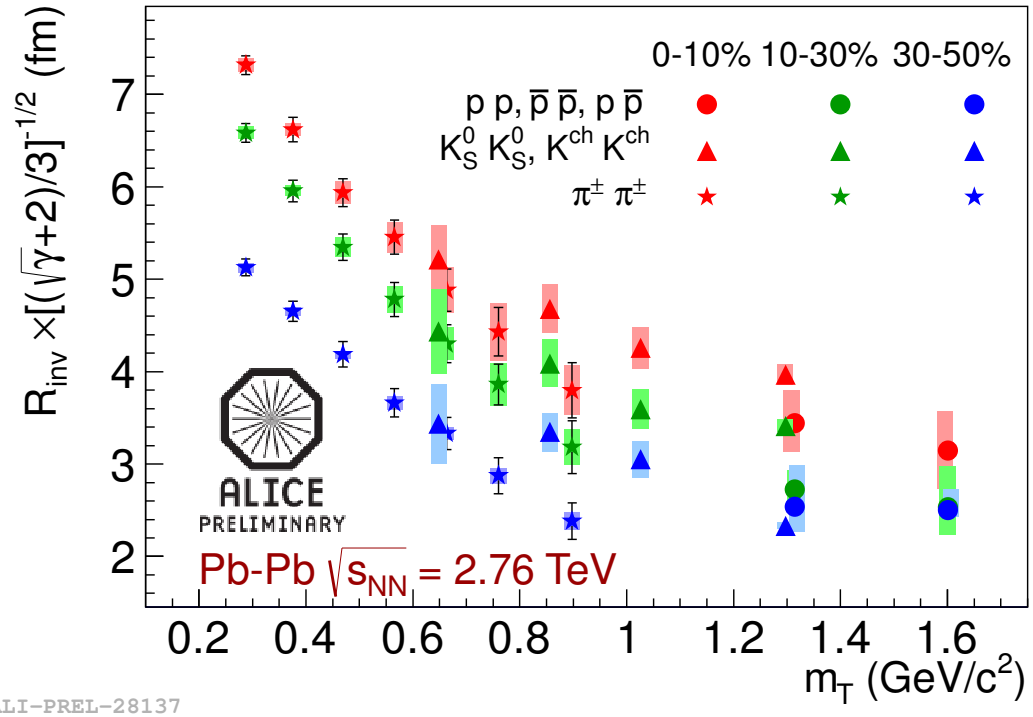

Fig. 37: m_{T} dependence of the radius parameter extracted from correlations of pions, charged kaons, neutral kaons and protons. Results for charged and neutral kaons as well as for (anti)protons are combined using weighted mean method (see text for details).

4 Summary

In summary, correlations of all combinations of pairs of protons and antiprotons have been measured in Pb–Pb collisions at $\sqrt{s_{\rm NN}} = 2.76$ TeV in the ALICE experiment. The femtoscopic parameters for the radius of the proton source are extracted from one-dimensional pp, $\bar{\rm p}\bar{\rm p}$ and $\rm p\bar{p}$ correlation functions. The fit includes final-state interactions and quantum statistics for identical pairs of (anti)protons. The fit takes into account residual correlations coming from pΛ system. Two-proton correlations show an increase of the radius with increasing multiplicity and slight decrease of the radius with increasing pair transverse momentum.

References

[1] The ALICE Collaboration: *Two-pion Bose-Einstein correlations in central PbPb collisions at* $\sqrt{s_{\rm NN}} = 2.76$ *TeV*; Phys.Lett.B696:328-337,2011

[2] Gos, H. P. for the STAR collaboration : *Proton - proton, anti-proton - anti-proton, proton - anti-proton correlations in Au+Au collisions measured by STAR at RHIC*; Eur.Phys.J. C49 (2007) 75-80

[3] Kisiel, A., Taluc, T., Broniowski W., Florkowski, W.; *THERMINATOR: THERMal heavy-IoN generATOR*; Comput.Phys.Commun. 174 (2006) 669-687

[4] Kisiel, A.: *CorrFit - a program to fit arbitrary correlation functions*; Nukleonika 49;Suppl 2:s81-s83 (2004)

[5] Lednicky, R.: *Finite-size effects on two-particle production in continuous and discrete spectrum*; Phys.Part.Nucl. 40 (2009) 307-352

[6] The LHC Computing Grid software development portal Savannah: `https://savannah.cern.ch/bugs/?func=detailitem&item_id=75267`

[7] Christian Klein-Boesing, private communication

[8] Malinina, L.: `https://indico.cern.ch/getFile.py/access?contribId=22&sessionId=6&resId=0&materialId=slides&confId=147108`

[9] Gramling, J.L. `http://indico.cern.ch/getFile.py/access?contribId=42&sessionId=16&resId=0&materialId=slides&confId=146554`